11. Walsh, D. M., and Selkoe, D. J. (2007) *J. Neurochem.* **101,** 1172–1184
12. Glabe, C. G. (2008) *J. Biol. Chem.* **283,** 29639–29643
13. Roychaudhuri, R., Yang, M., Hoshi, M. M., and Teplow, D. B. (2009) *J. Biol. Chem.* **284,** 4749–4753
14. Walsh, D. M., Lomakin, A., Benedek, G. B., Condron, M. M., and Teplow, D. B. (1997) *J. Biol. Chem.* **272,** 22364–22372
15. Podlisny, M. B., Ostaszewski, B. L., Squazzo, S. L., Koo, E. H., Rydell, R. E., Teplow, D. B., and Selkoe, D. J. (1995) *J. Biol. Chem.* **270,** 9564–9570
16. Lambert, M. P., Barlow, A. K., Chromy, B. A., Edwards, C., Freed, R., Liosatos, M., Morgan, T. E., Rozovsky, I., Trommer, B., Viola, K. L., Wals, P., Zhang, C., Finch, C. E., Krafft, G. A., and Klein, W. L. (1998) *Proc. Natl. Acad. Sci. U.S.A.* **95,** 6448–6453
17. Barghorn, S., Nimmrich, V., Striebinger, A., Krantz, C., Keller, P., Janson, B., Bahr, M., Schmidt, M., Bitner, R. S., Harlan, J., Barlow, E., Ebert, U., and Hillen, H. (2005) *J. Neurochem.* **95,** 834–847
18. Lesné, S., Koh, M. T., Kotilinek, L., Kayed, R., Glabe, C. G., Yang, A., Gallagher, M., and Ashe, K. H. (2006) *Nature* **440,** 352–357
19. Deshpande, A., Mina, E., Glabe, C., and Busciglio, J. (2006) *J. Neurosci.* **26,** 6011–6018
20. Chimon, S., Shaibat, M. A., Jones, C. R., Calero, D. C., Aizezi, B., and Ishii, Y. (2007) *Nat. Struct. Mol. Biol.* **14,** 1157–1164
21. Lacor, P. N., Buniel, M. C., Chang, L., Fernandez, S. J., Gong, Y., Viola, K. L., Lambert, M. P., Velasco, P. T., Bigio, E. H., Finch, C. E., Krafft, G. A., and Klein, W. L. (2004) *J. Neurosci.* **24,** 10191–10200
22. Kayed, R., Head, E., Thompson, J. L., McIntire, T. M., Milton, S. C., Cotman, C. W., and Glabe, C. G. (2003) *Science* **300,** 486–489
23. Lacor, P. N., Buniel, M. C., Furlow, P. W., Clemente, A. S., Velasco, P. T., Wood, M., Viola, K. L., and Klein, W. L. (2007) *J. Neurosci.* **27,** 796–807
24. Shankar, G. M., Bloodgood, B. L., Townsend, M., Walsh, D. M., Selkoe, D. J., and Sabatini, B. L. (2007) *J. Neurosci.* **27,** 2866–2875
25. Cleary, J. P., Walsh, D. M., Hofmeister, J. J., Shankar, G. M., Kuskowski, M. A., Selkoe, D. J., and Ashe, K. H. (2005) *Nat. Neurosci.* **8,** 79–84
26. Ashe, K. H. (2001) *Learn Mem.* **8,** 301–308
27. Hock, B. J., Jr., and Lamb, B. T. (2001) *Trends Genet.* **17,** S7–S12
28. Calhoun, M. E., Wiederhold, K. H., Abramowski, D., Phinney, A. L., Probst, A., Sturchler-Pierrat, C., Staufenbiel, M., Sommer, B., and Jucker, M. (1998) *Nature* **395,** 755–756
29. Bondolfi, L., Calhoun, M., Ermini, F., Kuhn, H. G., Wiederhold, K. H., Walker, L., Staufenbiel, M., and Jucker, M. (2002) *J. Neurosci.* **22,** 515–522
30. Shankar, G. M., Li, S., Mehta, T. H., Garcia-Munoz, A., Shepardson, N. E., Smith, I., Brett, F. M., Farrell, M. A., Rowan, M. J., Lemere, C. A., Regan, C. M., Walsh, D. M., Sabatini, B. L., and Selkoe, D. J. (2008) *Nat. Med.* **14,** 837–842
31. Kuo, Y. M., Emmerling, M. R., Vigo-Pelfrey, C., Kasunic, T. C., Kirkpatrick, J. B., Murdoch, G. H., Ball, M. J., and Roher, A. E. (1996) *J. Biol. Chem.* **271,** 4077–4081
32. Lue, L. F., Kuo, Y. M., Roher, A. E., Brachova, L., Shen, Y., Sue, L., Beach, T., Kurth, J. H., Rydel, R. E., and Rogers, J. (1999) *Am. J. Pathol.* **155,** 853–862
33. McLean, C. A., Cherny, R. A., Fraser, F. W., Fuller, S. J., Smith, M. J., Beyreuther, K., Bush, A. I., and Masters, C. L. (1999) *Ann. Neurol.* **46,** 860–866
34. Gómez-Isla, T., Hollister, R., West, H., Mui, S., Growdon, J. H., Petersen, R. C., Parisi, J. E., and Hyman, B. T. (1997) *Ann. Neurol.* **41,** 17–24
35. Morrison, J. H., and Hof, P. R. (1997) *Science* **278,** 412–419
36. Larrieu, S., Letenneur, L., Orgogozo, J. M., Fabrigoule, C., Amieva, H., Le Carret, N., Barberger-Gateau, P., and Dartigues, J. F. (2002) *Neurology* **59,** 1594–1599
37. Bouwman, F. H., Schoonenboom, S. N., van der Flier, W. M., van Elk, E. J., Kok, A., Barkhof, F., Blankenstein, M. A., and Scheltens, P. (2007) *Neurobiol. Aging* **28,** 1070–1074
38. Hoshi, M., Sato, M., Matsumoto, S., Noguchi, A., Yasutake, K., Yoshida, N., and Sato, K. (2003) *Proc. Natl. Acad. Sci. U.S.A.* **100,** 6370–6375
39. Lomakin, A., Chung, D. S., Benedek, G. B., Kirschner, D. A., and Teplow, D. B. (1996) *Proc. Natl. Acad. Sci. U.S.A.* **93,** 1125–1129
40. Demuro, A., Mina, E., Kayed, R., Milton, S. C., Parker, I., and Glabe, C. G. (2005) *J. Biol. Chem.* **280,** 17294–17300
41. Kuwano, R., Miyashita, A., Arai, H., Asada, T., Imagawa, M., Shoji, M., Higuchi, S., Urakami, K., Kakita, A., Takahashi, H., Tsukie, T., Toyabe, S., Akazawa, K., Kanazawa, I., and Ihara, Y. (2006) *Hum. Mol. Genet.* **15,** 2170–2182
42. Kayed, R., Head, E., Sarsoza, F., Saing, T., Cotman, C. W., Necula, M., Margol, L., Wu, J., Breydo, L., Thompson, J. L., Rasool, S., Gurlo, T., Butler, P., and Glabe, C. G. (2007) *Mol. Neurodegener.* **2,** 18
43. Mirra, S. S., Heyman, A., McKeel, D., Sumi, S. M., Crain, B. J., Brownlee, L. M., Vogel, F. S., Hughes, J. P., van Belle, G., and Berg, L. (1991) *Neurology* **41,** 479–486
44. Li, Y. T., Woodruff-Pak, D. S., and Trojanowski, J. Q. (1994) *Neurobiol. Aging* **15,** 1–9
45. Kepe, V., Huang, S. C., Small, G. W., Satyamurthy, N., and Barrio, J. R. (2006) *Methods Enzymol.* **412,** 144–160
46. Ince, P. G., and McKeith, I. G. (2003) in *Neurodegeneration: The Molecular Pathology of Dementia and Movement Disorders* (Dickson, D., ed) pp. 188–197, ISN Neuropath Press, Basel
47. Giasson, B. I., Lee, V. M.-Y., and Trojanowski, J. Q. (2004) in *The Neuropathology of Dementia* (Esiri, M., Lee, V. M.-Y., and Trojanowski, J. Q., eds) 2nd Ed., pp. 353–375, Cambridge University Press, Cambridge
48. Kosaka, K. (1990) *J. Neurol.* **237,** 197–204
49. Dezawa, M., Kanno, H., Hoshino, M., Cho, H., Matsumoto, N., Itokazu, Y., Tajima, N., Yamada, H., Sawada, H., Ishikawa, H., Mimura, T., Kitada, M., Suzuki, Y., and Ide, C. (2004) *J. Clin. Invest.* **113,** 1701–1710
50. De Felice, F. G., Velasco, P. T., Lambert, M. P., Viola, K., Fernandez, S. J., Ferreira, S. T., and Klein, W. L. (2007) *J. Biol. Chem.* **282,** 11590–11601
51. Zhao, W. Q., De Felice, F. G., Fernandez, S., Chen, H., Lambert, M. P., Quon, M. J., Krafft, G. A., and Klein, W. L. (2008) *FASEB J.* **22,** 246–260
52. Khosravani, H., Zhang, Y., Tsutsui, S., Hameed, S., Altier, C., Hamid, J., Chen, L., Villemaire, M., Ali, Z., Jirik, F. R., and Zamponi, G. W. (2008) *J. Cell Biol.* **181,** 551–565
53. Laurén, J., Gimbel, D. A., Nygaard, H. B., Gilbert, J. W., and Strittmatter, S. M. (2009) *Nature* **457,** 1128–1132
54. Klein, W. L., Krafft, G. A., and Finch, C. E. (2001) *Trends Neurosci.* **24,** 219–224
55. Bucciantini, M., Giannoni, E., Chiti, F., Baroni, F., Formigli, L., Zurdo, J., Taddei, N., Ramponi, G., Dobson, C. M., and Stefani, M. (2002) *Nature* **416,** 507–511
56. Walsh, D. M., Klyubin, I., Fadeeva, J. V., Cullen, W. K., Anwyl, R., Wolfe, M. S., Rowan, M. J., and Selkoe, D. J. (2002) *Nature* **416,** 535–539
57. Dickson, D. W., and Yen, S. H. (1989) *Neurobiol. Aging* **10,** 402–414
58. Terry, R. D., Masliah, E., Salmon, D. P., Butters, N., DeTeresa, R., Hill, R., Hansen, L. A., and Katzman, R. (1991) *Ann. Neurol.* **30,** 572–580
59. Thal, D. R., Rüb, U., Orantes, M., and Braak, H. (2002) *Neurology* **58,** 1791–1800
60. Hsiao, K., Chapman, P., Nilsen, S., Eckman, C., Harigaya, Y., Younkin, S., Yang, F., and Cole, G. (1996) *Science* **274,** 99–102
61. Kawarabayashi, T., Younkin, L. H., Saido, T. C., Shoji, M., Ashe, K. H., and Younkin, S. G. (2001) *J. Neurosci.* **21,** 372–381
62. Casas, C., Sergeant, N., Itier, J. M., Blanchard, V., Wirths, O., van der Kolk, N., Vingtdeux, V., van de Steeg, E., Ret, G., Canton, T., Drobecq, H., Clark, A., Bonici, B., Delacourte, A., Benavides, J., Schmitz, C., Tremp, G., Bayer, T. A., Benoit, P., and Pradier, L. (2004) *Am. J. Pathol.* **165,** 1289–1300
63. Oakley, H., Cole, S. L., Logan, S., Maus, E., Shao, P., Craft, J., Guillozet-Bongaarts, A., Ohno, M., Disterhoft, J., Van Eldik, L., Berry, R., and Vassar, R. (2006) *J. Neurosci.* **26,** 10129–10140
64. Pérez, M., Ribe, E., Rubio, A., Lim, F., Morán, M. A., Ramos, P. G., Ferrer, I., Isla, M. T., and Avila, J. (2005) *Neuroscience* **130,** 339–347
65. Wilcock, D. M., Gharkholonarehe, N., Van Nostrand, W. E., Davis, J., Vitek, M. P., and Colton, C. A. (2009) *J. Neurosci.* **29,** 7957–7965

THE JOURNAL OF BIOLOGICAL CHEMISTRY VOL. 284, NO. 8, pp. 4749–4753, February 20, 2009

Amyloid β-Protein Assembly and Alzheimer Disease*[S]

Published, JBC Papers in Press, October 9, 2008, DOI 10.1074/jbc.R800036200

Robin Roychaudhuri[‡], Mingfeng Yang[‡], Minako M. Hoshi[§], and David B. Teplow[‡1]

From the [‡]Department of Neurology, David Geffen School of Medicine, University of California, Los Angeles, California 90095 and the [§]Mitsubishi Kagaku Institute of Life Sciences, Tokyo 194-8511, Japan

The biochemistry of amyloid proteins has been a fascinating and important area of research because of its contribution to our understanding of protein folding dynamics and assembly and of the pathogenetic mechanisms of human disease. One such disease is AD,[2] the most common neurodegenerative disorder of aging. In AD, Aβ (Fig. 1*A*), which is expressed normally and ubiquitously throughout life as a 40–42-residue peptide, forms fibrils that deposit in the brain as "amyloid plaques." This pathologic deposition process led researchers to investigate fibril formation as a target for therapeutic intervention. In doing so, an increasing number of fibril precursors and non-fibrillar Aβ assemblies have been identified, the majority of which are neurotoxic. These findings have altered prevailing fibril-centered views of the pathobiology of amyloid diseases (1) and intensified efforts to understand the early folding and assembly dynamics of Aβ. In the discussion that follows, we seek to introduce the reader to the complex world of Aβ assembly and biological activity, a goal we hope will provide a conceptual framework upon which further knowledge or experimentation may be built.

Aβ Fibril Structure

The determination of the structure of fibrils has been an unusually difficult problem because Aβ belongs to a class of proteins that are "natively unfolded" (2) and preferentially form amyloid fibrils rather than protein crystals. This has precluded x-ray diffraction studies of full-length Aβ and made solution NMR studies problematic (3). Nevertheless, site-directed spin labeling and solid-state NMR studies have been informative. The former studies have revealed that Aβ fibrils comprise β-strands organized in a parallel, in-register fashion. The latter studies showed that in Aβ40 fibrils, residues 12–24 and 30–40 form parallel β-sheets and that these two β-strand segments are connected by a turn involving residues 25–29 (4). Hydrogen/deuterium exchange coupled with solution-state NMR revealed a similar, but distinct, segmental arrangement of β-strands within Aβ42 fibrils. Here, residues 18–26 and 31–42 form the β-strands. In both models, salt bridges between Asp^{23} and Lys^{28} stabilize the turn region connecting the two β-strands (2, 5). Similar findings have been obtained using other methods (5, 6).

Differences among the studies likely result from the examination of different peptides (Aβ40 *versus* Aβ42), the absence or presence of Met^{35}(O), or the conditions under which fibrils were formed. All these factors have been shown to affect significantly peptide assembly and biological activity (6, 7). Although no crystal structures have been determined with full-length Aβ, exciting work has been done on microcrystals formed by C-terminal peptides. These microcrystals yield diffraction patterns consistent with an in-register cross-β-organization of two interdigitated β-sheets. This "steric zipper" structure has been found in at least 13 other amyloid protein microcrystals (8). Whether steric zippers exists in Aβ fibrils is unclear.

Pathways of Peptide Assembly

How do monomers form fibrils? This question is fundamental to understanding fibrillogenesis and for identifying assembly steps that could be therapeutic targets. Influential early investigations promulgated the idea that Aβ assembly was a specific example of the general class of nucleation-dependent polymerization reactions (Fig. 1*B*). These reactions comprise a slow nucleation step, producing a "lag phase" during assembly monitoring, followed by a rapid fibril elongation step. Operating within this paradigm, nucleation (k_n) and elongation (k_e) rate constants for Aβ fibril formation were determined (9). However, continuing elucidation of this ostensibly classical polymerization process revealed unexpected complexity in the numbers and types ("on-pathway" or "off-pathway" for fibril formation) of assembly paths and the structures resulting therefrom (Fig. 1*C* and supplemental Table S1).

Protofibrils, Paranuclei, and Monomer Folds

Fig. 1*C* illustrates one pathway of fibril assembly. The penultimate fibril intermediate, the protofibril, was first identified more than a decade ago (10). Protofibrils were described as beaded chains, each bead of which was ~5 nm in diameter. The length of these structures generally was <150 nm. Kinetics and solution-phase AFM experiments showed that protofibrils matured into fibrils (10). To understand how protofibrils formed, methods were developed to determine quantitatively the oligomer size distribution in nascent Aβ preparations (11). In Aβ42 assembly, these experiments suggested that a pentamer or hexamer, the "paranucleus," was the basic unit of the protofibril and that the beaded chains comprising protofibrils formed by the self-association of paranuclei.

To understand the oligomerization process in atomic detail, computer simulations have been done (12). These studies yielded oligomer frequency distributions similar to those determined experimentally, but in addition provided high resolution

* This work was supported, in whole or in part, by National Institutes of Heath Grants NS038328 and AG027818. This work was also supported by the Jim Easton Consortium for Alzheimer's Drug Discovery and Biomarkers at UCLA and State of California Alzheimer's Disease Research Fund Grant 07-65806. This is the seventh article of eleven in the Thematic Minireview Series on the Molecular Basis of Alzheimer Disease. This minireview will be reprinted in the 2009 Minireview Compendium, which will be available in January, 2010.

[S] The on-line version of this article (available at http://www.jbc.org) contains supplemental Table S1 and additional references.

[1] To whom correspondence should be addressed. E-mail: dteplow@ucla.edu.

[2] The abbreviations used are: AD, Alzheimer disease; Aβ, amyloid β-protein; Met^{35}(O), Met^{35} sulfoxide; AFM, atomic force microscopy; CAA, cerebral amyloid angiopathy; ADDLs, Aβ-derived diffusible ligands.

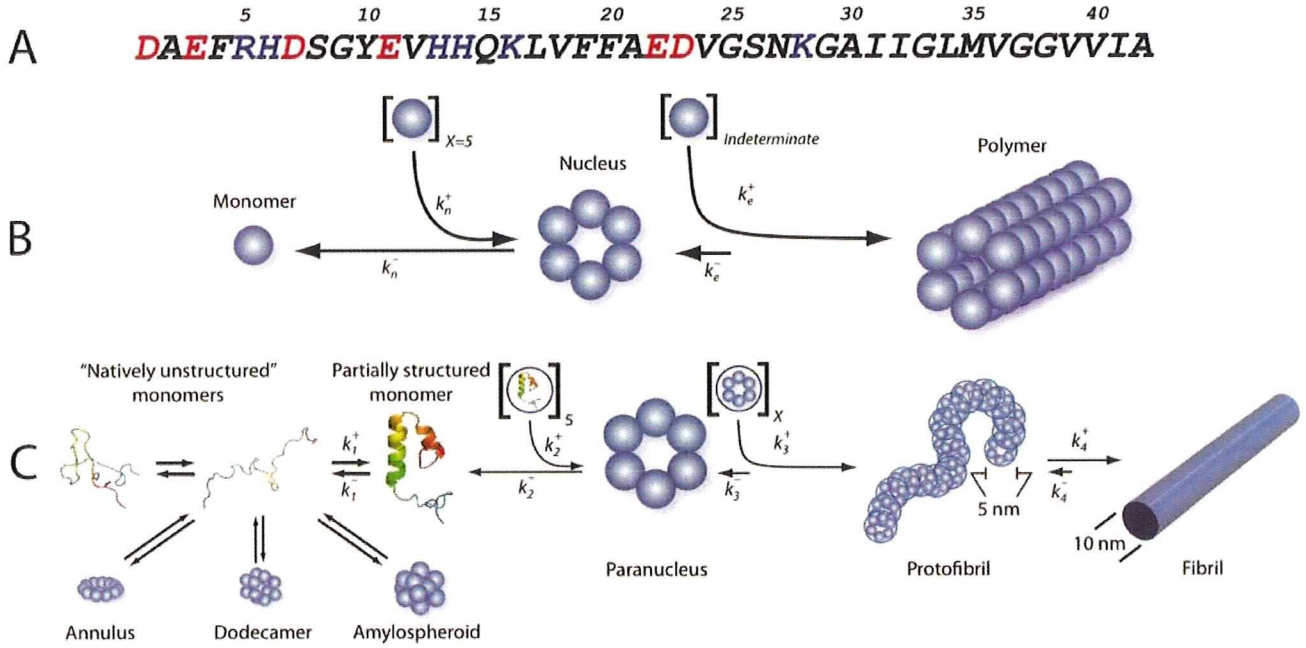

FIGURE 1. **Aβ assembly.** *A*, the sequence of Aβ42 is shown in one-letter amino acid code. The side chain charge at neutral pH is color-coded (*red*, negative; *blue*, positive). *B*, nucleation-dependent polymerization, reflecting the unfavorable self-association (rate constant $k_n^+ \ll k_n^-$) of *X* natively folded monomers (in this case, six total) to form a fibril nucleus and the favorable addition ($k_e^+ \gg k_e^-$) of a large indeterminate number of monomers to the nucleus (nascent fibril) during fibril elongation. *C*, Aβ self-assembly. Aβ belongs to the class of "natively disordered" proteins, existing in the monomer state as an equilibrium mixture of many conformers. On-pathway assembly requires the formation of a partially folded monomer that self-associates to form a nucleus for fibril elongation, a paranucleus (in this case, containing six monomers). Nucleation of monomer folding is a process distinct from fibril nucleation (50). Fibril nucleation is unfavorable kinetically ($k_2^+ \ll k_2^-$), which explains the lag phase of fibrillogenesis experiments, a period during which no fibril formation is apparent. Paranuclei self-associate readily ($k_3^+ \gg k_3^-$) to form protofibrils, which are relatively narrow (~5 nm), short (<150 nm), flexible structures. These protofibrils comprise a significant but finite number (*X*) of paranuclei. Maturation of protofibrils through a process that is kinetically favorable ($k_4^+ > k_4^-$) yields classical amyloid-type fibrils (~10-nm diameter, indeterminate (but often >1 μm) length). Other assembly pathways produce annular pore-like structures, globular dodecameric (and higher order) structures, and amylospheroids. Annuli and amylospheroids appear to be off-pathway assemblies.

conformational information. Aβ40 oligomers were more compact than Aβ42 oligomers due to increased conformational freedom of the Aβ42 N termini. This suggested that intermolecular interactions among Aβ42 N termini might facilitate the C-terminal interactions obligatory for fibril formation. The work also revealed the formation of a turn in Aβ42 at Gly^{37}-Gly^{38} that was not observed in Aβ40 and that thus could be critical in paranucleus formation.

The importance of the C terminus of Aβ in controlling Aβ assembly has also been revealed in experiments involving amino acid substitutions (11). Systematic alterations in residue 41 side chain hydrophobicity showed that Gly or Ala largely eliminated paranucleus formation, whereas amino acids with hydropathic characteristics similar to Ile had no effect. Elimination of the Ala^{42} side chain blocked paranucleus self-association, whereas insertion of larger apolar side chains facilitated the process. Similar studies examined Met^{35} polarity, an important question with respect to redox chemistry in AD (5, 11). In these experiments, oxidation of Met^{35} to Met^{35}(O) or Met^{35} sulfone had no effect on Aβ40 oligomerization, whereas Aβ42 paranucleus formation was abolished. Interestingly, the modified Aβ42 peptides oligomerized identically to Aβ40.

The relative importance of the C terminus in controlling Aβ assembly was also apparent in studies of Aβ40 and Aβ42 peptides containing substitutions linked to familial forms of AD or CAA. These substitutions ($Glu^{22} \rightarrow Gln$, $Glu^{22} \rightarrow Gly$, $Glu^{22} \rightarrow Lys$, and $Asp^{23} \rightarrow Asn$) produced oligomers of higher order when substituted in Aβ40 but had little effect on Aβ42 oligomerization. Removal of N-terminal residues Asp^1–Gly^9 in Aβ42 had no effect on its oligomer size distribution, whereas truncation of either the N-terminal two or four residues of Aβ40 produced higher-order oligomers. This observation was consistent with the aforementioned simulation data that suggested that collapse of the N terminus of Aβ40 on the oligomer surface might shield underlying hydrophobic regions of the oligomers that otherwise might interact to form higher-order assemblies (12). In fact, this process was observed in studies of the folding and assembly of urea-denatured Aβ (13). Aβ40 formed an unstable but largely collapsed monomeric species, whereas Aβ42 existed in a trimeric or tetrameric state (13).

The solvent inaccessibility of the Ala^{21}–Ala^{30} region of Aβ likely results from the formation of a turn-like structure that nucleates monomer folding (14). This decapeptide region initially was identified due to its resistance to proteolysis, a resistance that remained in the isolated decapeptide itself and that allowed NMR and computational determinations of its structure and dynamics (14). Most recently, thermodynamics studies showed that the turn is destabilized by amino acid substitutions that cause AD and CAA (15). Destabilization correlates with accelerated Aβ oligomerization and higher-order assembly and thus provides a mechanistic explanation for these familial forms of AD and CAA.

Other Assembly Pathways

The idea that an Aβ hexamer building block exists is intriguing because at least four other structures, ADDLs, Aβ*56, "globulomers," and "Aβ oligomers," comprise multiples of this basic unit (Fig. 1*C* and supplemental Table S1). ADDLs are dodecamers produced *in vitro* from Aβ42 using special solvent conditions and appear in AFM studies as globular structures with heights of 5–6 nm (16). Aβ*56 was identified in SDS extracts from brains of *Tg2576* transgenic mice (17). The "56" refers to the molecular weight of the oligomer, which is consistent with that of a dodecamer. The morphology of Aβ*56 is a prolate ellipsoid. A third type of dodecamer is the globulomer (so-called because it is a globular oligomer), which is formed by Aβ42 in the presence of SDS (18). Protease digestion, antibody binding, and mass spectrometry studies of globulomers suggest a structural model in which the hydrophobic C terminus (residues 24–42) forms a stable core and the more hydrophilic N terminus is on the surface. Although globulomers have substantial β-sheet content, presumably at the C terminus, they do not form fibrils and thus may be considered an off-pathway assembly (18). A larger species, the Aβ oligomer, also has been produced *in vitro* (19). Its molecular weight (~90,000) suggests that its assembly order is ~15–20, consistent with that of an octadecamer. In addition to assemblies with globular morphology, annular pore-like structures with diameters of 8–12 nm and pore sizes of 2–2.5 nm also have been described (10, 20).

The largest globular assemblies are amylospheroids and β-amyloid balls. Amylospheroids are off-pathway spheroidal structures with diameters of 10–15 nm that are formed by Aβ40 or Aβ42 (21). β-Amyloid balls are very large (20–200 μm) spheroidal structures formed only by Aβ40 at high concentration (300–600 μM) (22). Although such concentrations are non-physiological with respect to the average concentration of soluble Aβ *in vivo*, β-amyloid balls may be an interesting model of amyloid plaques or of the inclusion bodies formed in Parkinson and Huntington diseases and in the transmissible spongiform encephalopathies.

Assembly Complexity and Provenance

The complexity of Aβ assembly complicates the determination of precursor-product relationships. For example, are the different dodecameric assemblies discussed above really different, or are they all the same entity described in different ways by different investigators? Do the different larger spheroidal assemblies form from the same hexamer building blocks that produce dodecamers and thus belong on the same pathway? We do not know, but the answers to these questions are important because they have implications for the development of therapeutic agents targeting critical steps in the assembly pathways. For example, recent work has shown that compounds exist that can efficiently inhibit fibril formation or oligomerization, but not both (23). The distinction is critical if one assembly is benign and the other toxic.

Aβ Assembly and Disease

Thus far, we have discussed basic aspects of the physical biochemistry of Aβ assembly. However, the most fundamental biological question is, "what is the relationship between Aβ assemblies and AD?" Strong linkage exists between amyloid formation *per se* and disease (for a comprehensive review, see Ref. 24), and this linkage formed, in part, the foundation for the "amyloid cascade hypothesis," which posited that amyloid fibril formation was the key pathogenetic process in AD (25). As discussed above, elucidation of the mechanisms of fibril formation unexpectedly revealed a broad range of fibrillar and nonfibrillar structures (supplemental Table S1). Aβ oligomers appear to be particularly important because they are potent neurotoxins and are isolable from AD patients, and their concentrations correlate positively with neuropathology *in vivo*. These facts have produced a fundamental paradigm shift resulting in a revised amyloid cascade hypothesis (1, 20, 26), one that posits the primacy of oligomeric forms of Aβ in AD causation.

A substantial experimental corpus exists demonstrating that "Aβ" is neurotoxic (27). However, it was not until approximately a decade ago, with the discovery and characterization of protofibrils and ADDLs, that a more structurally precise definition of Aβ could be made, one that in turn enabled more precise structure-neurotoxicity correlations to be established (16, 28). Each new assembly subsequently discovered also was toxic. An important goal of current research is to better define the mechanisms of this toxicity, a variety of which we now discuss.

Membrane Effects

Aβ is an amphipathic peptide (Fig. 1*A*). The side chains of 16 of the first 28 residues are polar; 12 are charged at neutral pH. The remaining 12 (Aβ40) or 14 (Aβ42) side chains are apolar. Structures such as these can form micelles (29) or interact with membranes directly. Recent work has shown that Aβ40 inserts into membranes of hippocampal neurons from AD brains (30). Membrane insertion can perturb plasma membrane structure and function. For example, conformational analysis of the C-terminal domain of Aβ (residues 29–40/2) has shown it to have properties similar to those of fusion peptides of viral proteins. Insertion of these fragments in a tilted manner in the membrane is thought to disrupt the parallel symmetry of the fatty acyl chains, altering the curvature of the membrane surface and destabilizing the membrane. Consistent with this prediction, Aβ(22–42) induces membrane fusion and permeabilizes lipid vesicles that mimic neuronal membranes (31).

Aβ oligomers have also been shown to increase the conductance of lipid bilayers and living cell membranes by lowering the "dielectric barrier," possibly by increasing the membrane dielectric constant, introducing localized structural defects, or thinning the membrane (thereby facilitating charge translocation across the bilayer) (32). These effects may be related to oligomer-induced release of membrane components, including cholesterol, phospholipids, and monosialogangliosides, which in turn may lead to tau hyperphosphorylation and neurodegeneration (30, 33).

Structured membrane reorganization may also occur. Aβ40 oligomers form cation-sensitive ion channels in neuronal plasma membranes and liposomes (30, 34). These channels may comprise four to six subunits, each of which is an Aβ oligomer of order four to six, and thus the channels comprise a

total of 16–36 Aβ monomers. The channels are quasi-stable, suggesting that channel formation is a dynamic process (31). For example, Arispe *et al.* (31) have shown that Aβ40 channel activity in planar lipid bilayers results in spontaneous transitions to higher conductances. AFM images of Aβ-treated reconstituted bilayers have revealed disk-like structures with pore-like concavities of 8–12-nm outside diameter and 1–2-nm inside diameter. However, pore formation remains a contentious issue. Some believe that Aβ oligomer-mediated interference with the surface packing of lipid headgroups effectively thins the membrane, reduces effective membrane conductance, and may produce the appearance of pores. Time-lapse AFM experiments have revealed that Aβ aggregates ~500 nm in size form along the edges of bilayer defects, a result that could be misinterpreted as pore formation (35). Consistent with this interpretation are recent results suggesting that oligomers alter membrane conductivity without forming discrete pores (32).

We note that two general classes of Aβ/membrane interaction may occur: 1) nonreceptor-mediated structural interactions of the type discussed above; and 2) specific receptor-mediated interactions. These latter interactions may involve fibrillar and oligomeric forms of Aβ that act either as agonists or antagonists. Many membrane Aβ receptors have been identified (30), but the important question that remains unanswered is whether these interactions are physiologically relevant or serendipitous.

Metals, Aggregation, and Radicals

Evidence exists that metals are involved in the pathogenesis of AD. However, this is a contentious issue that remains unresolved. We present here a number of prominent mechanistic hypotheses.

In vitro results indicate that physiological concentrations of Zn^{2+} and Cu^{2+} can accelerate Aβ aggregation and increase Aβ toxicity (36, 37). Aβ has a strong positive reduction potential and displays high-affinity binding for Cu^{2+}, Zn^{2+}, and Fe^{3+} ions (34). Solution-state NMR and EPR have suggested that the three His residues in Aβ, His^6, His^{13}, and His^{14}, coordinate Cu^{2+}. This metalloenzyme-like complex has been proposed to catalyze Fenton chemistry (Equation 1),

$$Me^{n+} + H_2O_2 \rightarrow Me^{(n+1)+} + OH^{\bullet} + OH^{-} \quad \text{(Eq. 1)}$$

which yields toxic hydroxyl ($OH^{\bullet}$) and peroxide ($OOH^{\bullet}$) radicals. Fe^{2+} is also thought to participate in this chemistry. In addition to its postulated catalytic role in Fenton chemistry, it has been suggested that Aβ-linked inhibition of catalase increases H_2O_2 production (Equation 2) (38).

$$Me^{(n+1)+} + H_2O_2 \rightarrow Me^{n+} + OOH^{\bullet} + H^{+} \quad \text{(Eq. 2)}$$

A second center for redox chemistry is Met^{35} (39). The generation of reactive oxygen species by Aβ requires reduction of Cu^{2+} or Fe^{3+}, a reaction that may proceed through the oxidation of Met^{35} to its corresponding sulfide radical cation. Cu^{+} or Fe^{2+} produced in this way may react with molecular oxygen and biological reducing agents (*e.g.*; cholesterol, vitamin C, or catecholamine) to yield H_2O_2 and the starting Cu^{+} cation (40). The H_2O_2 thus produced can further oxidize Met^{35} to its sulfoxide form and also react with superoxide anion ($O_2^{\bullet-}$) in a Haber-Weiss reaction to produce $OH^{\bullet}$ (Equation 3).

$$O_2^{\bullet-} + H_2O_2 \rightarrow OH^{\bullet} + OH^{-} + O_2 \quad \text{(Eq. 3)}$$

Interestingly, the Met^{35}(O) and Met^{35} sulfone forms of Aβ do not assemble as does the wild-type peptide (11, 41). Hou *et al.* (41) have reported that oxidation of Met^{35} to Met^{35}(O) significantly reduces the rate of amyloid formation and alters fibril morphology. Bitan and Teplow (11) reported similar findings and found that Met^{35}(O) Aβ42 does not form paranuclei, but rather oligomerizes similarly to Aβ40. These *in vitro* observations are consistent with the strong negative correlation that exists between oxidative damage and Aβ deposition in AD (11, 39).

Murakami *et al.* (42) have proposed that Tyr^{10} is also involved in redox chemistry. They suggested that H_2O_2 produced by Aβ-metal complexes oxidizes Tyr^{10} to produce the tyrosyl radical, which then attacks the thioether of Met^{35} and yields an *S*-oxidized radical cation. A turn at Gly^{38}–Val^{39} brings the C-terminal carboxylate anion proximate to the radical, stabilizing it and simultaneously creating a hydrophobic subdomain facilitating peptide oligomerization, fibril formation, and longer lasting oxidative stress.

Mitochondrial Effects

Mitochondrial dysfunction has been linked directly to the aging process (43), a process that is the largest single risk factor for AD. Exacerbation of age-related dysfunction by toxic Aβ assemblies may explain the linkage of both age and Aβ to AD. Increasing evidence suggests that Aβ-induced mitochondrial dysfunction does in fact occur. The interaction of full-length Aβ or truncated forms with mitochondria causes potent inhibition of electron transport chain enzyme complexes and reductions in the activities of tricarboxylic acid cycle enzymes, leading to inhibition of ATP production, mitochondrial swelling, cytochrome *c* release, caspase activation, transition pore opening, increased mitochondrial reactive oxygen species production, and decreased mitochondrial membrane potential and respiration rates (43, 44). Complexation of Aβ with Aβ-binding alcohol dehydrogenase, a mitochondrial matrix enzyme, or with endoplasmic reticulum-associated Aβ-binding protein also produces this type of damage (45).

Apoptosis

A common final pathway of Aβ-induced neuronal dysfunction is apoptosis. This pathway is particularly likely to occur following mitochondrial compromise. Aβ40 and Aβ42 oligomers also have been shown recently to activate sphingomyelinases, which results in apoptotic cell death through a redox-sensitive cytosolic phospholipase A_2/arachidonic acid-dependent pathway (46). In rat hippocampal neuron cultures, activation of ERK1/2 (extracellular signal-regulated kinase-1/2) by Aβ oligomers results in caspase-3 activation, tau cleavage, dysregulation of cell structure, and finally apoptosis (47). Transforming growth factor-β1 has been found to exacerbate Aβ-induced toxicity through Smad7 and β-catenin interac-

tions and nuclear localization. Aβ40 also can activate the NF-κB apoptosis pathway by selectively inducing the nuclear translocation of the NF-κB p65 and p50 subunits. For this reason, p65 and p50 have been suggested as AD therapeutic targets. The connection of apoptosis with Aβ assemblies is supported by the observation that up-regulation in neurons of peroxisome proliferator-activated receptor-γ, which increases expression of the anti-apoptotic protein Bcl-2, protects these cells against Aβ-induced toxicity (48).

An Explication

The impetus for studies of Aβ structure, dynamics, and bioactivity has been the causal link of Aβ to AD. The result of these studies has been an extraordinary expansion of knowledge. The rapidly increasing number of clinical trials of mechanistically novel AD therapies suggests that this knowledge has been of value (49). However, a consensus does not exist regarding either the biophysical or biological behavior of Aβ. For academics, rigorous experiments done in well controlled systems provide reliable, although not necessarily clinically relevant, information. However, for AD patients, their families, and the treating clinicians, relevance is paramount. For their sake, it is hoped that the information presented here will stimulate current and especially new researchers to conceive of novel experimental approaches seeking to answer three fundamental questions. 1) Is Aβ, in fact, the proximate etiologic agent of AD; 2) if so, what is the structure of the proximate neurotoxic Aβ assembly; and 3) if not, what is?

REFERENCES

1. Kirkitadze, M. D., Bitan, G., and Teplow, D. B. (2002) *J. Neurosci. Res.* **69,** 567–577
2. Nelson, R., and Eisenberg, D. (2006) *Curr. Opin. Struct. Biol.* **16,** 260–265
3. Teplow, D. B. (2006) *Methods Enzymol.* **413,** 20–33
4. Tycko, R. (2006) *Methods Enzymol.* **413,** 103–122
5. Finder, V. H., and Glockshuber, R. (2007) *Neurodegener. Dis.* **4,** 13–27
6. Fändrich, M. (2007) *CMLS Cell. Mol. Life Sci.* **64,** 2066–2078
7. Kodali, R., and Wetzel, R. (2007) *Curr. Opin. Struct. Biol.* **17,** 48–57
8. Sawaya, M. R., Sambashivan, S., Nelson, R., Ivanova, M. I., Sievers, S. A., Apostol, M. I., Thompson, M. J., Balbirnie, M., Wiltzius, J. J. W., McFarlane, H. T., Madsen, A., Riekel, C., and Eisenberg, D. (2007) *Nature* **447,** 453–457
9. Teplow, D. B. (1998) *Amyloid* **5,** 121–142
10. Caughey, B., and Lansbury, P. T. (2003) *Annu. Rev. Neurosci.* **26,** 267–298
11. Bitan, G., and Teplow, D. B. (2004) *Acc. Chem. Res.* **37,** 357–364
12. Urbanc, B., Cruz, L., Yun, S., Buldyrev, S. V., Bitan, G., Teplow, D. B., and Stanley, H. E. (2004) *Proc. Natl. Acad. Sci. U. S. A.* **101,** 17345–17350
13. Chen, Y.-R., and Glabe, C. G. (2006) *J. Biol. Chem.* **281,** 24414–24422
14. Teplow, D. B., Lazo, N. D., Bitan, G., Bernstein, S., Wyttenbach, T., Bowers, M. T., Baumketner, A., Shea, J.-E., Urbanc, B., Cruz, L., Borreguero, J., and Stanley, H. E. (2006) *Acc. Chem. Res.* **39,** 635–645
15. Grant, M. A., Lazo, N. D., Lomakin, A., Condron, M. M., Arai, H., Yamin, G., Rigby, A. C., and Teplow, D. B. (2007) *Proc. Natl. Acad. Sci. U. S. A.* **104,** 16522–16527
16. Lambert, M. P., Barlow, A. K., Chromy, B. A., Edwards, C., Freed, R., Liosatos, M., Morgan, T. E., Rozovsky, I., Trommer, B., Viola, K. L., Wals, P., Zhang, C., Finch, C. E., Krafft, G. A., and Klein, W. L. (1998) *Proc. Natl. Acad. Sci. U. S. A.* **95,** 6448–6453
17. Lesné, S., Koh, M. T., Kotilinek, L., Kayed, R., Glabe, C. G., Yang, A., Gallagher, M., and Ashe, K. H. (2006) *Nature* **440,** 352–357
18. Gellermann, G. P., Byrnes, H., Striebinger, A., Ullrich, K., Mueller, R., Hillen, H., and Barghorn, S. (2008) *Neurobiol. Dis.* **30,** 212–220
19. Deshpande, A., Mina, E., Glabe, C., and Busciglio, J. (2006) *J. Neurosci.* **26,** 6011–6018
20. Haass, C., and Selkoe, D. J. (2007) *Nat. Rev. Mol. Cell Biol.* **8,** 101–112
21. Hoshi, M., Sato, M., Matsumoto, S., Noguchi, A., Yasutake, K., Yoshida, N., and Sato, K. (2003) *Proc. Natl. Acad. Sci. U. S. A.* **100,** 6370–6375
22. Westlind-Danielsson, A., and Arnerup, G. (2001) *Biochemistry* **40,** 14736–14743
23. Necula, M., Kayed, R., Milton, S., and Glabe, C. G. (2007) *J. Biol. Chem.* **282,** 10311–10324
24. Sipe, J. C. (ed) (2005) *Amyloid Proteins: The Beta Sheet Conformation and Disease,* Wiley-VCH, Weinheim, Germany
25. Hardy, J. (1996) *Ann. Med.* **28,** 255–258
26. Hardy, J., and Selkoe, D. J. (2002) *Science* **297,** 353–356
27. Yankner, B. A., and Lu, T. (2009) *J. Biol. Chem.* **284,** 4755–4759
28. Walsh, D. M., Hartley, D. M., Kusumoto, Y., Fezoui, Y., Condron, M. M., Lomakin, A., Benedek, G. B., Selkoe, D. J., and Teplow, D. B. (1999) *J. Biol. Chem.* **274,** 25945–25952
29. Lomakin, A., Chung, D. S., Benedek, G. B., Kirschner, D. A., and Teplow, D. B. (1996) *Proc. Natl. Acad. Sci. U. S. A.* **93,** 1125–1129
30. Verdier, Y., Zarndi, M., and Penke, B. (2004) *J. Pept. Sci.* **10,** 229–248
31. Arispe, N., Diaz, J. C., and Simakova, O. (2007) *Biochim. Biophys. Acta* **1768,** 1952–1965
32. Sokolov, Y., Kozak, J. A., Kayed, R., Chanturiya, A., Glabe, C., and Hall, J. E. (2006) *J. Gen. Physiol.* **128,** 637–647
33. Tashima, Y., Oe, R., Lee, S., Sugihara, G., Chambers, E. J., Takahashi, M., and Yamada, T. (2004) *J. Biol. Chem.* **279,** 17587–17595
34. Kawahara, M., Arispe, N., Kuroda, Y., and Rojas, E. (1997) *Biophys. J.* **73,** 67–75
35. Green, J. D., Kreplak, L., Goldsbury, C., Blatter, X. L., Stolz, M., Cooper, G. S., Seelig, A., Kistler, J., and Aebi, U. (2004) *J. Mol. Biol.* **342,** 877–887
36. Jun, S., and Saxena, S. (2007) *Angew. Chem. Int. Ed. Engl.* **46,** 5251–5263
37. Bush, A. I. (2003) *Trends Neurosci.* **26,** 207–214
38. Behl, C., Davis, J. B., Lesley, R., and Schubert, D. (1994) *Cell* **77,** 817–827
39. Butterfield, D. A. (2003) *Curr. Med. Chem.* **10,** 2651–2659
40. Crouch, P. J., Harding, S.-M. E., White, A. R., Camakaris, J., Bush, A. I., and Masters, C. L. (2008) *Int. J. Biochem. Cell Biol.* **40,** 181–198
41. Hou, L., Kang, I., Marchant, R. E., and Zagorski, M. G. (2002) *J. Biol. Chem.* **277,** 40173–40176
42. Murakami, K., Irie, K., Ohigashi, H., Hara, H., Nagao, M., Shimizu, T., and Shirasawa, T. (2005) *J. Am. Chem. Soc.* **127,** 15168–15174
43. Crouch, P. J., Cimdins, K., Duce, J. A., Bush, A. I., and Trounce, I. A. (2007) *Rejuvenation Res.* **10,** 349–357
44. Mancuso, C., Scapagini, G., Curr, D., Stella, A. M. G., Marco, C. D., Butterfield, D. A., and Calabrese, V. (2007) *Front. Biosci.* **12,** 1107–1123
45. Chen, J. X., and Yan, S. D. (2007) *J. Alzheimer's Dis.* **12,** 177–184
46. Malaplate-Armand, C., Florent-Bchard, S., Youssef, I., Koziel, V., Sponne, I., Kriem, B., Leininger-Muller, B., Olivier, J.-L., Oster, T., and Pillot, T. (2006) *Neurobiol. Dis.* **23,** 178–189
47. Chong, Y. H., Shin, Y. J., Lee, E. O., Kayed, R., Glabe, C. G., and Tenner, A. J. (2006) *J. Biol. Chem.* **281,** 20315–20325
48. Fuenzalida, K., Quintanilla, R., Ramos, P., Piderit, D., Fuentealba, R. A., Martinez, G., Inestrosa, N. C., and Bronfman, M. (2007) *J. Biol. Chem.* **282,** 37006–37015
49. Yamin, G., Ono, K., Inayathullah, M., and Teplow, D. B. (2008) *Curr. Pharm. Des.* **14,** 3231–3246
50. Lazo, N. D., Grant, M. A., Condron, M. C., Rigby, A. C., and Teplow, D. B. (2005) *Protein Sci.* **14,** 1581–1596

the role of proteasome in the proteolysis of Aβ is still uncertain. To explore the role of proteasome in Aβ accumulation of AD pathologies, we investigated here the influence of proteasome inhibition on Aβ production and the underlying mechanisms in rats. **Methods:** We injected bilaterally lactacystin, an irreversible inhibitor of proteasome, into the rat hippocampus and employed Western blotting, immunohistochemistry, and enzyme linked immunosorbent assay (ELISA) to measure the alterations of Aβ production and the possible mechanisms in rats. **Results:** We observed the following results in our experiment. (1) Lactacystin inhibited the proteasome activities; (2) After proteasome inhibition, the level of Aβ40 and Aβ42 were both increased by ELISA, and Aβ fragments were also increased by Wesstern blotting and immunohistochemstry with 4G8 and 6E10; (3) APP levels including full length and C-Terminal fragment cleaved by β-secretase (CTF-β) were elevated upon proteasome inhibition; (4) BACE1, PS-1 and PS-2 were increased at the different time points, witch suggested that β-secretase and γ-secretase activity were increased after proteasome inhibition. **Conclusions:** We conclude that proteasome inhibition led to the increase of Aβ production through elevating APP level and the β- and γ-secretase activities in rat brain.

P1-151 EFFECT OF TARGETING $I_2^{PP\text{-}2A}$ WITH SIRNAS ON ALZHEIMER-LIKE PATHOLOGY IN TG2576 MICE

Wei Wei, *Tongji Medical College, Huazhong University of Science and Technology, Wuhan, China. Contact e-mail: rocky1240@163.com*

Background: In Alzheimer's disease, increased inhibitor-2 of protein phosphatase-2A ($I_2^{PP\text{-}2A}$) level has been associated with decreased protein phosphatase-2A activity. Thus, reduction of $I_2^{PP\text{-}2A}$ level could play a vital role in the treatment of Alzheimer's disease. Here, to explore the role of $I_2^{PP\text{-}2A}$ in Alzheimer's disease pathology, we investigate the effect of $I_2^{PP\text{-}2A}$ reduction on Aβ, tau, memory and the underlying mechanisms in 12-months Tg2576 mice (Tg-mice). **Methods:** We injected the lentiviral vectors (LV)-si$I_2^{PP\text{-}2A}$ expressing siRNA targeting $I_2^{PP\text{-}2A}$ to lower the $I_2^{PP\text{-}2A}$ levels into the left hippocampus and right cerebralventricle, and employed Western blotting, immunohistochemistry, Morris water maze to measure the changes of Aβ, tau phosphorylation, as well as the learning and memory in the Tg-mice. **Results:** We found that firstly, $I_2^{PP\text{-}2A}$ level was decreased after injection of LV- si$I_2^{PP\text{-}2A}$ in the left hippocampus and the right cortex of the Tg-mice; Secondly, with $I_2^{PP\text{-}2A}$ reduction, the level of Aβ, APP and the APP phosphorylation were decreased; Thirdly, tau hyperphosphorylation at Ser199/202, Ser214 and Ser396 sites was reduced, and the levels of PP-$2A_C$, phosphorylated PP-$2A_C$ at Tyr-307 and GSK-3β at Ser9 were all increased, which suggested that PP-2A activity was increased while GSK-3β activity was decreased, and these maybe contribute to the reduction of tau phosphorylation at those sites. Fourthly, after injection of LV- si$I_2^{PP\text{-}2A}$, the learning and memory retention abilities were also improved in the Tg-mice, and the c-fos was increased simultaneously. **Conclusions:** Down regulation of $I_2^{PP\text{-}2A}$ with siRNAs reduces the Aβ load through decreasing APP level and its phosphorylation, and tau phosphorylation partially through increasing PP-2A activity and/or decreasing GSK-3β activity, and ameliorates the learning and memory ability of Tg-mice.

P1-152 THE CHANGING OF DISTRIBUTION AND LOCATION OF NEUROGLOBIN IN TG2576 TRANSGENIC MOUSE

Liming Chen[1,2], [1]*Key Laboratory of Neurological Diseases, wuhan, China;* [2]*Tongji Medical College, Huazhong University of Science and Technology, Department of Pathophysiology, Wuhan, China. Contact e-mail: 51651286@qq.com*

Background: Neuroglobin (Ngb), a recently discovered vertebrate globin expressed predominantly in the brain. Ngb is similar to myoglobin and hemoglobin and shares their capability for oxygen binding. It has thus been proposed to act as an oxygen reservoir or combats reactive oxygen species. It was also known to protect cells against amyloid toxicity and to attenuate the AD phenotype of transgenic mice. But the mechanism of this neuroprotection is unclear. **Methods:** We investigated the ngb expression pattern in the Tg2576 mouse brain using immunohistochemistry and immunofluorescence. Selecting mouse as four group from juvenile to senium.(about 3month ,8month,12month,18month). **Results:** The immunohistochemistry and immunofluorescence shows the neuroglobin positive neuron to dedrease gradually from four aging model in hippocampus CA3, but not cortex. The construction of neuron fiber deranged gradually also. **Conclusions:** In hippocampus CA3, the overexpression app may effect the production of neuroglobin.neuroglobin may as a new biomarker to diagnose alzheimer disease in future.

P1-153 LGI3 ASSOCIATES WITH ASTROGLIAL RESPONSE AGAINST ABETA AND ACCUMULATES IN AGED MONKEY BRAINS

Sachi Okabayashi[1], Nobuyuki Kimura[2], [1]*The Corporation for Production and Research of Laboratory Primates, Tsukuba-shi, Japan;* [2]*Tsukuba Primate Research Center, National Institute of Biomedical Innovation, Ibaraki, Japan. Contact e-mail: okarin@primate.or.jp*

Background: The leucine-rich glioma inactivated (LGI) family of genes encodes a leucine-rich repeat (LRR) protein, proteins that are thought to be specifically involved in protein-protein and protein-matrix interactions. Since amyloid beta peptide (Aβ) has been previously shown to induce the expression of another LRR-encoding gene in neural cells, we assessed how Aβ affects LGI gene expression in rat primary cerebral cortical cultures and astrocyte cultures. **Results:** Both RT-PCR and Western blot analyses revealed that Aβ robustly induced the expression of LGI3 in rat astrocyte cultures coincidentally with the up-regulation of glial fibrillary acidic protein (GFAP) and apolipoprotein E (ApoE). Immunocytochemistry showed that LGI3 colocalized with Aβ at plasma membranes and also with internalized Aβ in astrocytes. These findings suggest that activated LGI3 may be involved in the astroglial response against Aβ. Furthermore, we examined in monkey brains of various ages the *in vivo* relationship between Aβ and LGI3. Immunohistochemistry showed that LGI3 was present in almost all cortical neurons and astrocytes, and mainly localized to nuclei and plasma membranes. In aged monkey brains, both LGI3 and Aβ colocalized on/near plasma membranes, forming large, diffuse clusters. Moreover, LGI3 localized in lipid rafts, colocalizing with endocytosis-associated proteins, which also accumulated near the plasma membranes of neurons in aged monkey brains. **Conclusions:** These findings indicate that LGI3 is not only associated with Aβ but also with endocytosis system in brain, and that aging caused these proteins to accumulate on/near plasma membranes.

P1-154 IDENTIFICATION OF AMYLOSPHEROID-BINDING PROTEINS FROM MATURE NEURONS AS A MOLECULAR TARGET OF NEUROTOXICITY INDUCED BY NONFIBRILLAR AB ASSEMBLIES

Yasuki Kitamura, Masako Yanazawa, Michio Sato, Akane Ito, **Minako M. Hoshi**, *Mitsubishi Kagaku Institute of Life Sciences, Tokyo, Japan. Contact e-mail: minhoshi@mitils.jp*

Background: The conversion of amyloid β-protein (Aβ) into neurotoxic Aβ assemblies is suggested to be a key initiating event of Alzheimer's disease. Studies suggest that Aβ assemblies induce synaptic impairment and neuronal loss through interaction with neurons. To elucidate molecular mechanisms of Aβ neurotoxicity, we have first identified 10-15-nm spherical Aβ assemblies termed "amylospheroids" (ASPDs) (~130 kDa in mass) as neurotoxic in-vitro assemblies. We recently demonstrated their in vivo existence and their high neurotoxicity (A.N., D.B.T., M.H., unpublished data). Our previous studies revealed that ASPDs cause degeneration of mature neurons by their binding to neuronal surface, suggesting that binding of ASPDs to putative toxic target(s) on mature neuronal surface might trigger signals leading to cell death. We therefore aim to isolate ASPD-binding proteins from mature neurons. **Methods:** Biotin-labeled ASPDs were prepared from 50 μM solutions of Aβ1-42 containing a small amount of biotinylated Aβ1-40 by slowly rotating the solutions. The biotin-labeled ASPDs were separated from monomers and other smaller Aβ assemblies using 100-kDa molecular-weight-cut-off filters. Mature rat hippocampal neuronal cultures were incubated briefly with the isolated biotin-labeled ASPDs. Extracts containing the biotin-labeled ASPD-putative-ASPD-binding protein complexes were obtained by

solubilizing the above neuronal cells using mild detergents. The biotin-labeled ASPD-putative-ASPD-binding protein complexes were isolated using streptavidin beads. The isolated ASPD-binding proteins were separated by SDS-PAGE, visualized using silver stain. **Results:** We first examined whether ASPD-binding proteins are present or not in mature neuron-derived extracts using far-Western blotting. We could detect some bands that were specifically detected by anti-ASPD antibodies but not by an anti-Aβ antibody using ASPDs as ligands. These bands were absent in extracts derived from immature neurons or from non-neuronal cells. We next attempted to isolate ASPD-binding proteins using biotin-labeled ASPDs as baits. We optimized the experimental conditions for isolating the biotin-labeled ASPD-putative-ASPD-binding protein complexes from mature neuron-derived extracts and finally succeeded to detect the bands of the putative ASPD-binding proteins in SDS-PAGE analysis, some of which were identical to the bands detected by far-Western blotting. **Conclusions:** We thus isolated the candidates for the neurotoxic targets for ASPDs from mature neurons. Further analysis using mass spectrometry is proceeding to characterize the isolated proteins.

P1-155 EXCLUSION OF PHOSPORYLATED APP CTFS FROM MEMBRANE REGION RICH IN ACTIVE γ-SECRETASE

Takahide Matsushima, Tadashi Nakaya, Toshiharu Suzuki, *Hokkaido University, Sapporo, Japan. Contact e-mail: matusima@pharm.hokudai.ac.jp*

Background: In neuron, mature APP695 (mAPP, N- and O-glycosylated form) is phosphorylated at Thr668 within the motif 667-VTPEER-672 of cytoplasmic domain. Function of APP can be modified by cytoplasmic conformational change induced with the phosphorylation (reviewed in *J. Biol. Chem.* [2008] 283 29633-29637). Several reports indicated that phosphorylation or amino acid substitutions for Thr668 of APP could regulate the cleavage by β-secretase and/or γ-secretase, or that phosphorylation at Thr668 has been up-regulated in AD brains. Contrary to these observation, a mutant mice carrying amino acid substitution of Ala for Thr668 (A/A mutant), which mimicked non-phosphorylated APP, did not influence in APP processing in brain. Thus the participation of phosphorylation in APP metabolism is still under consideration. We herein report the role of APP phosphorylation in γ-site cleavage of APP. **Methods:** Levels of phosphorylated APP CTFs (pCTFs) and nonphosphorylated CTFs (nCTFs) in mice brain membrane were examined by Western blotting and their relative amounts were quantified. The brain samples were subjected to *in vitro* γ-secretase assay and the cleavage of pCTFs was compared to that of nCTFs. **Results:** In CTFβ, C99 and C89, the phosphorylated form was dominant compared to nonphosphorylated forms, while both pCTF and nCTF were even in quantity for CTFα, C83. When the membrane fraction including these CTFs was assayed for γ-secretase cleavage, the cleavage of pCTFs was significantly lower compared to that of nCTFs in spite of kinetic equivalence of pCTFs and nCTFs for susceptibility to γ-secretase. **Conclusions:** *In vitro* γ-cleavage assay of CTFs indicates that phosphorylated and non-phosphorylated CTFs were kinetically equivalent substrates for γ-secretase. However, more nCTFs were likely to be cleaved rather than pCTFs. This indicates that phosphorylation for Thr668 regulates the localization of CTFs instead of a direct inhibition of γ-cleavage. The pCTFs may be located at a distance from the active γ-secretase in the membrane, while non-phosphorylated CTFs are located close to the active enzyme. The model what we have proposed differes from the interpretation that phosphorylation of CTFs directly interferes or facilitates in cleavage by γ-secretase.

P1-156 THE PATHOGENIC I716F AMYLOID PRECURSOR PROTEIN (APP) MUTATION LEADS TO A REDUCED PROTEIN PROCESSING AND A VERY AGGRESSIVE EARLY-ONSET ALZHEIMER'S DISEASE

Cristina Guardia-Laguarta[1], Marta Pera[1], Jordi Clarimon[1], Albert Llado[2], Raquel Sánchez-Valle[2], Jose Luis Molinuevo[2], Teresa Gómez-Isla[1], Rafael Blesa[1], Isidre Ferrer[3], Alberto Lleo[1], *[1]Hospital Sant Pau, Barcelona, Spain; [2]Hospital Clinic, Barcelona, Spain; [3]Hospital de Bellvitge, Barcelona, Spain. Contact e-mail: cguardia@santpau.es*

Background: Previous studies suggest that a mutation in the codon 716 of the amyloid precursor protein (APP) leads to familial early onset Alzheimer's disease (EOAD) with an age of onset in the mid 50s. We report a novel mutation in APP (I716F) in a patient with an onset of 31 years. We investigate in detail the clinical, neuropathological and biochemical effects of this mutation. **Methods:** Neuropathological examination was performed using specific antibodies against amyloid-β , tau/phospho-tau, α -sinuclein, TDP-43, and GFAP. cDNA constructs encoding APPV717I and APPI716F were generated by site-directed mutagenesis. CHO cells were transfected with wtAPP, APPV717I or APPI716F, and Aβ 40 and Aβ 42 levels were measured by ELISA. APP C-terminal fragments (CTFs) were measured by Western blot. We measured the APP intracellular domain (AICD) in an in vitro cell-free assay. Finally, γ -secretase activity was measured by a fluorometric assay in cell lysates, and brain samples from the proband, AD patients and healthy controls. **Results:** The proband had a diagnosis of EOAD with an age of onset of 31 (age of death of 36). The father had developed EOAD with an age of onset of 35. The neuropathological examination of the proband showed abundant diffuse amyloid plaques, mainly stained for Aβ42, and widespread neurofibrillary pathology corresponding to a stage VI of Braak. Lewy bodies and aberrant neurites were observed in the amygdala. CHO cells transfected with the APP I716F and V717I mutations showed a marked increase of the Aβ42/40 ratio in the media compared to wtAPP. Both mutations led to a decrease in AICD production and reduced γ-secretase activity. APP CTFs levels were increased in cells transfected with both mutations as well as in the proband's brain sample. **Conclusions:** The APP I716F mutation is associated with a very early age of onset and aggressive neuropathological phenotype. Our data indicates that this mutation, as well as the V717I APP mutation, leads to an increased $A\beta_{42/40}$ ratio but also to a reduced APP proteolysis by γ -secretase. This suggests an additional mechanism by which mutations around γ -secretase cleavage site may lead to AD.

P1-157 γ-SECRETASE SUBSTRATES APP, NOTCH1 AND CD44 SHOW DISTINCT PROCESSING IN NPC CELLS

Martina Malnar[1], Harald Steiner[2], Sven Lammich[2], Silva Hecimovic[1], *[1]Rudjer Boskovic Institute, Zagreb, Croatia; [2]Ludwig-Maximilians-University, Munich, Germany. Contact e-mail: martina.malnar@irb.hr*

Background: It has been previously demonstrated that NPC1 dysfunction, that causes Niemann Pick type C disease (NPC), results in altered APP processing leading to increased levels of C99 and amyloid-β peptide (Aβ). To elucidate whether the Aβ increase upon NPC1 loss of function is due to a common mechanism of altered γ-secretase processing, we analyzed the levels of β-like peptides and intracellular domains (ICDs) of APP, Notch1 and CD44 in wt (CHOwt) and NPC cells (CHO NPC1-null). **Methods:** The cells were transiently transfected with C99, Flag-Next or CD44ΔE-Flag constructs (all C-terminal myc tagged). In order to detect β-peptides, media were collected, cleared and immunoprecipitated using appropriate antibodies. Immunoprecipitates were subjected to SDS-PAGE on Schägger gels and blotted onto nitrocellulose membranes. The membranes were probed with antibody FLAG-M2 (CD44-β and Notch1-β) or 6E10 (Aβ). For detection of ICDs, cell lysates were subjected to SDS-PAGE, blotted on PVDF membranes and immunoblotted with antibody 9E10. **Results:** In contrast to the markedly increased levels of Aβ, we did not observe an increase in Notch-β and CD44-β peptides in NPC compared to wt cells. Our observation that AICD levels were similar in wt and NPC cells, suggests that cholesterol accumulation upon NPC1 dysfunction may specifically affect γ-secretase cleavage at γ40/42-site and not γ-secretase cleavage at the ϵ-site. In addition, the levels of Notch1-ICD (NICD) and CD44-ICD were similar between wt and NPC cells, further supporting the hypothesis that γ-secretase processing of Notch1 and CD44 is not altered in NPC cells. **Conclusions:** We found that NPC1 loss specifically affects Aβ levels and not the levels of other γ-secretase generated β-like peptides. These results suggest that there is not a common mechanism of γ-secretase cleavage that would result in similar γ-secretase processing of APP, Notch1 and CD44 in NPC cells. This finding supports a model of distinct processing pathways of γ-secretase substrates, indicating that designing an

THE JOURNAL OF BIOLOGICAL CHEMISTRY VOL. 284, NO. 48, pp. 33139–33150, November 27, 2009

Triple *N*-Glycosylation in the Long S5-P Loop Regulates the Activation and Trafficking of the Kv12.2 Potassium Channel*[S]

Received for publication, May 26, 2009, and in revised form, September 1, 2009 Published, JBC Papers in Press, October 6, 2009, DOI 10.1074/jbc.M109.021519

Kentaro Noma[‡1], Kazushi Kimura[§], Keiichiro Minatohara[‡], Hisako Nakashima[§], Yasuaki Nagao[§], Akira Mizoguchi[§], and Yoshinori Fujiyoshi[‡2]

From the [‡]Department of Biophysics, Graduate School of Science, Kyoto University, Oiwake, Kitashirakawa, Sakyo-ku, Kyoto 606-8502, Japan and the [§]Department of Neural Regeneration and Cell Communication, Mie University Graduate School of Medicine, Tsu, Mie 514-8507, Japan

Mammalian voltage-dependent potassium (Kv) channels regulate the excitability of nerve and muscle cells. Kv12.2 features the longest S5-P loop among all known mammalian Kv channels with the most *N*-linked glycosylation sites (three sites). Despite its unique structural features, Kv12.2 is not well characterized. Because glycosylation plays important roles in the folding, trafficking, and function of various Kv channels, we focused on the *N*-glycosylation of Kv12.2. We show that Kv12.2 is *N*-glycosylated in Chinese hamster ovary (CHO) cells and in cultured neurons as well as in the mouse brain. As an effect of *N*-glycosylation on the function of Kv12.2, we demonstrate that removal of sugar chains causes a depolarizing shift in the steady-state activation without a significant reduction in current amplitude. Unlike the previously reported shift for *Shaker*-type Kv channels, this shift does not appear to be due to negatively charged sialic acid residues in the sugar chains. We next examined the trafficking in CHO cells to address whether the unglycosylated Kv12.2 channels are utilized *in vivo*. Although double mutants, retaining only one glycosylation site, are trafficked to the surface of CHO cells irrespective of the position of the glycosylated site, unglycosylated channels are not trafficked to the cell surface. Furthermore, we could not detect unglycosylated channels in the mouse brain. Our data suggest that only glycosylated Kv12.2 channels show proper voltage dependence and are utilized *in vivo*.

Mammalian voltage-dependent potassium (Kv)[3] channels are multisubunit membrane proteins that regulate the excitability of nerve and muscle cells (1). The channels are composed of four α-subunits, with each α-subunit containing six membrane-spanning segments (S1-S6) (Fig. 1*A*). The S1-S4 helices function as the voltage sensor, whereas the S5-S6 helices together with a pore helix between them tetramerize to form a central ion-conducting pore. Mammalian Kv channels constitute a large superfamily and are categorized into groups termed Kv1.x ~ Kv12.x according to their primary sequences (2, 3). Kv12.2, also known as ether-a-go-go-like 2 (Elk2) or KCNH3, belongs to the ether-a-go-go (EAG) family, which comprises the ether-a-go-go (Eag, Kv10.x), ether-a-go-go-related gene (Erg, Kv11.x), and ether-a-go-go like (Elk, Kv12.x) subfamilies (4, 5). In mouse, rat, and human, Kv12.2 mRNA is specifically expressed in the brain (6–8). In the human brain expression levels of Kv12.2 mRNA are high in the cerebral cortex, hippocampus, amygdala, caudate, and nucleus accumbens (9). In these parts of the brain the level of Kv12.2 mRNA was found to be as high as 15~30% that of ribosomal protein RS9, a housekeeping gene (9). Unlike Kv5.x, Kv6.x, Kv8.x, and Kv9.x, which function as modifiers for other Kv channels (10), Kv12.2 can produce a functional channel on its own when heterologously expressed (6–8, 11). In addition, human Kv12.2 may be implicated in epilepsy (12). These findings suggest that Kv12.2 is likely to play important roles in the mammalian brain. Among all known mammalian Kv channels, Kv12.2 has the longest extracellular S5-P loop located between S5 and the pore helix (Fig. 1*A*, *right panel*) and the largest number of (*i.e.* three) *N*-glycosylation consensus sequences in the S5-P loop (Fig. 1*B*). Despite these findings and unique structural features, Kv12.2 has not yet been well characterized at the protein level (10).

Many Kv channels undergo *N*-linked glycosylation, which begins with the co-translational addition of a core glycan to a lumenal-exposed asparagine residue that is part of a consensus sequence. As the proteins progress through the Golgi apparatus, enzymes modify the sugar chains, resulting in high mannose, hybrid, or complex oligosaccharides (13, 14). *N*-Glycosylation generally promotes proper folding, increases trafficking and stability, and modifies the function of Kv channels (15–20), but the positions and roles of *N*-glycosylation vary among Kv channels. With the exception of Kv1.6, *Shaker* type Kv1.x channels have a single glycosylation consensus sequence in a loop located between helices S1 and S2 (Fig. 1*A*, *left panel*), and in some Kv1.x channels removal of the *N*-linked glycans results in a positive shift of the activation curve (15, 19). It has been suggested that this effect is due to negatively charged sialic acid residues in the sugar chains. In contrast, despite the fact that EAG-type Kv channels have one or more *N*-glycosylation sites adjacent to the pore region (Fig. 1*B*), only a few studies have addressed the role of *N*-glycosylation in the functional regula-

* This work was supported by Grants-in-aid for Specially Promoted Research and the Japan New Energy and Industrial Technology Development Organization.

[S] The on-line version of this article (available at http://www.jbc.org) contains supplemental Figs. 1–3.

[1] Supported by a fellowship from the Japan Society for the Promotion of Science.

[2] To whom correspondence should be addressed. Tel.: 81-75-753-4216; Fax: 81-75-753-4218; E-mail: yoshi@em.biophys.kyoto-u.ac.jp.

[3] The abbreviations used are: Kv channels, voltage-dependent potassium channels; CHO, Chinese hamster ovary; Eag, ether-a-go-go; EGFP, enhanced green fluorescent protein; Elk, ether-a-go-go-like; Erg, ether-a-go-go-related gene; HERG, human ether-a-go-go-related gene; PB, phosphate buffer; PBS, phosphate-buffered saline; Endo H, endoglycosidase H; PNGase F, peptide *N*-glycosidase F.

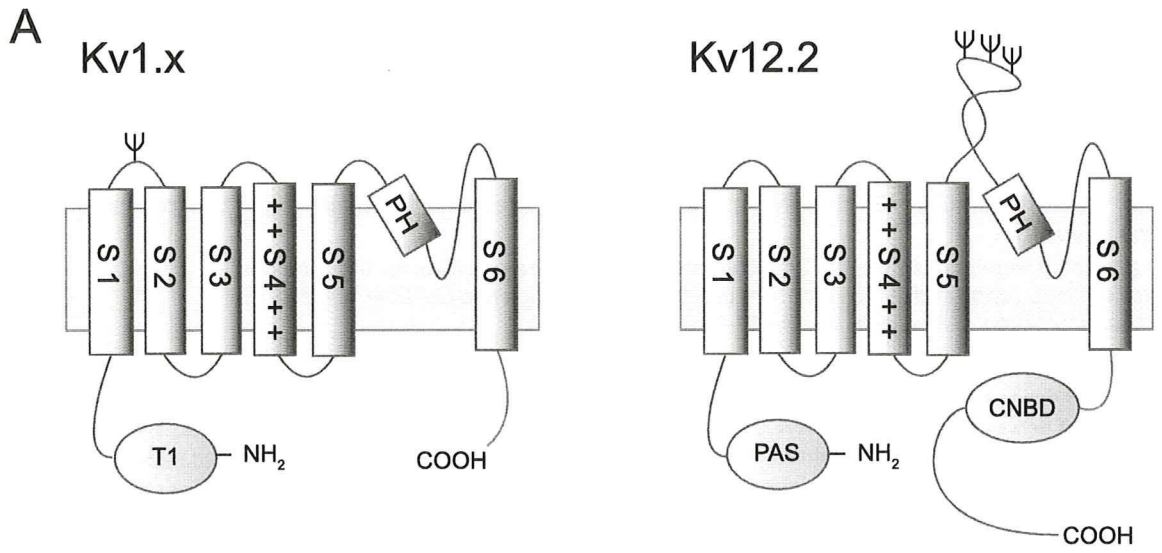

B

		10 (392)	20 (402)	30 (412)	40 (422)	50 (432)
Kv12.2	**(Elk)**	**QQEIENSESELPEIGWLQELARRLETPYYLVSRSPDGGNSSGQSENCSSS**				
Kv1.2	(Shaker)	ADERDSQFPS				
Kv1.4	(Shaker)	ADEPTTHFQS				
Kv2.1	(Shab)	KDEDDTKFKS				
Kv3.1	(Shaw)	RIGAQPNDPSASEHTHFKN				
Kv4.1	(Shal)	KGTSKTNFTS				
Kv10.1	(Eag)	DYEIFDEDTKTIRNNSWLYQLALDIGTPYQFNGSGSGKWEGGPSKNSV				
Kv11.1	(Erg)	NMEQPHMDSHIGWLHNLGDQIGKPYNSSGLGGPSIKDK				
Kv12.1	(Elk)	KMEREDNSLLKWEVGWLHELGKRLESPYYGNNTLGGPSIRSA				
Kv12.3	(Elk)	RREMEANDPLLWDIGWLHELGKRLEEPYVNGSAGGPSRRSA				
Drosophila Elk		VKEYEWFPESNIGWLQLLAERKNASVAILTTAET				
Danio Elk1		RKEMETNASGAWDIGWLHELGKRLDKPYMNSTFGGPSVRSA				

		50 (432)	60 (442)	70 (452)	80 (462)
Kv12.2	**(Elk)**	**SSSSGSGGGGGSEANGTGLELLGGPSLRSA**			

FIGURE 1. **Topological model and amino acid sequence of S5-P loops of various voltage-dependent potassium channels.** *A*, the proposed topology of the Kv1.x and Kv12.2 monomers is shown. Kv channels have six transmembrane segments (S1-S6). Helix S4 contains positively charged residues, indicated by +. The predicted *N*-linked glycosylation sites are indicated by Ψ. Kv1.x channels have an N-terminal tetramerization domain (*T1*), and single *N*-glycosylation site between helix S1 and S2 with the exception of Kv1.6. Kv12.2 channels have an N-terminal Per-Arnt-Sim (*PAS*) domain and a C-terminal cyclic nucleotide biding domain (*CNBD*). Kv12.2 has three *N*-glycosylation sites in a particularly long extracellular S5-P loop between helix S5 and the pore helix (*PH*). *B*, shown are amino acid sequences of the predicted S5-P loops of the mouse Kv, fruit fly (*Drosophila melanogaster*) Elk, and zebrafish (*Danio rerio*) Elk1 channels. The *names* in *parentheses* refer to the subfamilies containing the corresponding mouse Kv channels. Elk, Eag, and Erg are subfamilies of the EAG family. *White letters in black boxes* indicate the predicted *N*-linked glycosylation consensus sequence Asn-Xaa-(Ser/Thr) in which Xaa can be any amino acid except proline. The *numbers in parentheses above the sequences* indicate the positions of the residues in Kv12.2.

tion of these channels (18). The analysis of Kv12.2 provides insights into the role of *N*-glycans in the function of channels of the EAG family.

Regulation of trafficking to the cell surface, where Kv channels are generally expressed, is another important role of the *N*-glycosylation of these channels (21, 22). The effect of glycosylation on trafficking varies between Kv channels. Glycosylation of Kv1.1 does not affect the trafficking of the channel (16, 23). It has been suggested that both glycosylated and unglycosylated Kv1.1 could be utilized *in vivo* and that differences in the degree of glycosylation increase the functional diversity of the channels, possibly modifying cell excitability (24). In contrast, the human Erg (HERG or Kv11.1) channel requires glycosylation for proper cell surface expression (20, 25). Mutations that prevent glycosylation of the HERG protein cause a cardiac disorder known as long QT syndrome type 2 (20). These data suggest isoform-specific differences in the sensitivity of potassium channel trafficking to *N*-linked glycosylation.

Here we present the evidence that Kv12.2 channels are expressed and *N*-glycosylated in the mouse brain and that *N*-glycosylation is essential for proper function of EGFP-Kv12.2 expressed in Chinese hamster ovary (CHO) cells. Furthermore, by a systematic mutational analysis of the three glycosylation sites of Kv12.2, our study provides insight into how glycosylation regulates the trafficking of Kv channels.

EXPERIMENTAL PROCEDURES

Cloning and Plasmid Construction—Kv12.2 cDNA was isolated by PCR from a mouse brain library using Prime STAR GXL DNA polymerase (Takara Bio Inc., Otsu, Japan) and specific primers (5′-primer, 5′-GCTAGCGCCACCATGCCGGCCATGCGGGGGCTCCTG-3′; 3′-primer, 5′-TTGCGGCCGCTCAGACCCCTGTGCCTTCTTCCTGGGT-3′). A NheI-Kozak sequence was introduced at the 5′ end of the PCR product and a NotI restriction site at the 3′ end, and the construct was cloned into the pGEM T-easy cloning vector (Promega). With the exception of two silent mutations (G1161A and G2682A), our mouse Kv12.2 cDNA sequence is identical to GenBank™ accession number NM_010601.3 but differs slightly from GenBank™ accession number AF109143 (8). The NheI-NotI fragment from the Kv12.2 cloning vector was ligated into digested pcDNA3.1(+) vector (Invitrogen). For the EGFP-Kv12.2 construct, EGFP was isolated by PCR from the pEGFP C2 vector (Clontech) and ligated to the 5′ end of Kv12.2 in the pcDNA3.1(+) vector. EGFP-Kv12.2 substitution mutants were generated from EGFP-Kv12.2 with the QuikChange II site-directed mutagenesis kit (Stratagene, Birmingham, AL) according to the manufacturer's instructions. To avoid undesired mutations, after point mutations were introduced into the EGFP-Kv12.2 construct, the fragments were sequenced and ligated into confirmed vectors. For expression of EGFP-Kv12.2 in primary cultured neurons, the EGFP-Kv12.2 fragment was cloned into the pCA mammalian expression vector under the chicken β-actin promoter. The pCA-based EGFP-Kv12.2 vector resulted in higher protein expression in cultured neurons than the pcDNA3.1-based vector.

CHO Cell Culture and Transfection—CHO K1 cells were grown in Dulbecco's modified Eagle's medium (Sigma) supplemented with 10% heat-inactivated fetal bovine serum (BioWhittaker), 50 units/ml penicillin, and 50 μg/ml streptomycin at 37 °C in a humidified 5% CO_2 atmosphere. CHO-K1 cells in a 35-mm Petri dish were transfected with a mixture containing 1.5 μg of the EGFP-Kv12.2 expression plasmid and 5 μl of Lipofectamine (Invitrogen) according to the manufacturer's instructions. For transfection of CHO-K1 cells in 60-mm Petri dishes, twice as much EGFP-Kv12.2 expression plasmid and Lipofectamine were used.

Patch Clamp Recordings and Data Analysis—Whole-cell Kv12.2 currents were recorded 36–48 h after transfection at 25 °C. Cells were voltage-clamped with an EPC10 amplifier (HEKA Elektronik, Lambrecht, Germany). Patch pipette resistances were 2–3.5 megaohms. The external solution contained 10 mM HEPES-NaOH (pH 7.4), 112 mM NaCl, 40 mM KCl, 1.5 mM $CaCl_2$, 1 mM $MgCl_2$, and 10 mM glucose. The internal pipette solution contained 10 mM HEPES-KOH (pH 7.3), 10 mM NaCl, 130 mM potassium gluconate, 1.3 mM $CaCl_2$, 2 mM $MgCl_2$, 10 mM EGTA, and 1 mM ATP. To generate the steady-state activation curve, an established tail current protocol was used (6, 8, 11). Inward tail currents were elicited by voltage steps at −120 mV after conditioning pulses from −80 to 80 or 100 mV for 3 s. The small inward tail current for the conditioning pulse of −80 mV was subtracted from all measured currents. The peak amplitudes of the tail currents were normalized and plotted against the conditioning potential. The data points were fitted with a Boltzmann function of the form $g = g_{max}/1 + \exp(-(V_m - V_{1/2})/k)$, where g_{max} is the maximum conductance, $V_{1/2}$ is the voltage of half-maximal activation, V_m is the applied membrane potential of the conditioning pulse, and k is the slope factor. Data are usually given as the mean value ± the S.E. The channel activity was evaluated from the average peak amplitude of tail currents at −100 mV after a conditioning potential of 120 mV for 500 ms.

Primary Hippocampal Cell Culture—E18 rat hippocampi dissected in Hanks' balanced salt solution without calcium and magnesium were treated with 0.25% trypsin for 15 min at 37 °C and dispersed with a constricted Pasteur pipette (20 times) to produce a homogeneous suspension. The isolated neurons were washed with Hanks' balanced salt solution without calcium and magnesium and subjected to electroporation using the Nucleofector system (Amaxa Inc., Gaithersburg, MD). Briefly, 2~3 × 10^6 dissociated neurons were spun down at 100 × *g* for 3 min at 4 °C, resuspended in 100 μl of rat neuron Nucleofector solution kept at room temperature, combined with 3 μg of plasmid DNA, transferred into a cuvette, and electroporated using program O-03 of the Amaxa system. Transfected neurons (200,000 ~ 400,000 per 60-mm dish) were plated in tissue culture dishes coated with poly-L-lysine (Sigma) in neurobasal medium (Invitrogen) containing 1/50 volume of B27 (Invitrogen) and 1 mM GlutaMAX (Invitrogen). The neurons were maintained at 37 °C in a humidified 5% CO_2 atmosphere for 14 days and used for immunoblot analysis.

Antibody against the Very C Terminus of Kv12.2—Antibody against the Kv12.2 protein was raised using as antigen a peptide corresponding to its very C terminus (residues 1081–1095). The synthetic peptide was conjugated to keyhole limpet hemocyanin and injected into rabbits to generate polyclonal antibodies according to standard protocol. The antibody was affinity-purified from the rabbit serum and used for immunoblotting (anti-Kv12.2(1081)). The anti-Kv12.2(787) antibody was raised against a peptide corresponding to C-terminal residues 787–800 using the same method described for anti-Kv12.2(1081).

Immunoblot Analysis—48 h after transfection, CHO cells were washed with phosphate-buffered saline (PBS; 8.1 mM Na_2HPO_4, 1.5 mM KH_2PO_4, 137 mM NaCl, 2.7 mM KCl; Takara Bio, Inc.) and harvested. To solubilize the Kv12.2 protein, cell pellets were suspended in solubilization buffer (1% *n*-dodecyl-β-D-maltopyranoside (Dojindo Laboratories, Kumamoto, Japan) in 50 mM Tris-HCl (pH 7.5), 150 mM NaCl, 1 mM EDTA) supplemented with 1/100 volume of protease inhibitor mixture (Nacalai Tesque, Inc., Kyoto, Japan) and 1 mM phenylmethylsulfonyl fluoride and incubated for 30 min on ice. After removing cell debris by centrifugation at 20,000 × *g* for 30 min, the supernatant was resolved by SDS-PAGE (7.5% gel). The lanes were transferred to a polyvinylidene difluoride membrane (Bio-

Rad), which was incubated with anti-Kv12.2 antibody at 2.5 μg/ml for about 12 h at 4 °C. The antibody was detected by horseradish peroxidase-conjugated secondary antibody (Promega) and visualized using ECL Advance (Amersham Biosciences). The bands were quantified using an LAS-3000 image analyzer (FUJI FILM).

At 14 days *in vitro* hippocampal neurons were washed with PBS, harvested, and treated like CHO cells except that for solubilization of neurons radioimmune precipitation assay buffer was used (1% Nonidet P-40, 0.5% sodium deoxycholate, 0.1% SDS in 50 mM Tris-HCl (pH 7.5), 150 mM NaCl, 1 mM EDTA) supplemented with 1/100 volume of protease inhibitor mixture (Nacalai Tesque) and 1 mM phenylmethylsulfonyl fluoride.

For the detection of native Kv12.2, crude membrane fractions were prepared from freshly dissected whole brains of mice of different ages (embryonic 17 day, postnatal day 5 (PD5), P13, or adult (P210)). Crude membrane fractions prepared from livers of adult mice were used as control. Samples were homogenized in homogenization buffer (0.32 M sucrose, 10 mM HEPES-NaOH (pH 7.0), 0.1 mM $CaCl_2$, 1 mM $MgCl_2$, 1/100 volume of protease inhibitor mixture). The homogenate was centrifuged at 1500 × *g* for 10 min to remove cell debris, and the supernatant was centrifuged at 13,500 × *g* for 10 min. The pellet was resuspended in homogenization buffer and stored at −80 °C. Protein content was determined using the DC Protein Assay system (Bio-Rad) with bovine serum albumin as standard. 20 μg of protein was added to reducing SDS sample buffer, boiled for 3 min at 95 °C, and analyzed by immunoblotting as described above.

Enzymatic Deglycosylation—*n*-Dodecyl-β-D-maltopyranoside or radioimmune precipitation assay buffer-solubilized proteins from transfected cells or crude membrane fractions from mouse tissues were denatured by boiling for 3 min at 95 °C in buffer containing 1% β-mercaptoethanol and 0.5% SDS. The denatured samples were treated with 50 units/μl Endo H (New England Biolabs) or 50 units/μl PNGase F (New England Biolabs) for 1 h at 37 °C. The reaction was stopped by adding an equal volume of 2× SDS sample buffer and boiling the samples for 3 min at 95 °C.

Tunicamycin Treatment—8–10 h after transfection with the EGFP-Kv12.2 construct, CHO cells were treated with 50 μg/ml tunicamycin (Sigma) or an equal volume of dimethyl sulfoxide (DMSO) as control. CHO cells were cultured for an additional ~36 h and analyzed by immunoblot or patch clamp experiments.

PNGase F or Neuraminidase Treatment of Live CHO Cells—For PNGase F treatment of live CHO cells, EGFP-Kv12.2-transfected cells in a 35-mm tissue culture dish were washed 3 times with PBS containing 1 mM $MgCl_2$ and 1 mM $CaCl_2$ (PBS-MC) and incubated with 1 ml of PBS-MC containing 0, 500, 1000, 2500, or 5000 units of PNGase F for 1 h at 37 °C. The removal of sugar chains was monitored by immunoblotting. Cells treated with 1000 units of PNGase F were used for patch clamp recordings within 1 h after treatment. Neuraminidase treatment was performed as described for PNGase F using 0, 50, or 100 units in 1 ml of PBS-MC for immunoblot experiments and 50 units for patch clamp experiments.

Fluorescence Microscopy and Immunoelectron Microscopy—For confocal immunofluorescence microscopy, CHO cells were cultured in eight-well culture slides (Nunc, Naperville, IL). 36–48 h after transfection fluorescence images were acquired at room temperature with an FV1000 confocal laser-scanning microscope (Olympus, Tokyo, Japan).

For immunoelectron microscopy, CHO cells were fixed 48 h after transfection for 2 h at room temperature with 2% paraformaldehyde (Merck) in 0.1 M phosphate buffer (PB) at pH 7.5 containing 20 μM (*p*-amidinophenyl)methanesulfonyl fluoride hydrochloride. After washing with 100 mM PB, cells were incubated for 15 min in 20% Blockace (Dainippon Pharmaceutical, Osaka, Japan) in 100 mM PB containing 20 μM (*p*-amidinophenyl)methanesulfonyl fluoride hydrochloride and 0.005% saponin (Merck). Cells were then incubated overnight at 4 °C with anti-green fluorescent protein polyclonal antibody (Abcam, Cambridge, MA) diluted 1:1000 in dilution buffer (100 mM PB containing 5% Blockace and 0.05% saponin (Merck)). After washing with washing buffer (100 mM PB containing 0.05% saponin (Merck)), cells were incubated for 2 h at room temperature with 1-nm gold-conjugated goat anti-rabbit IgG (Nanogold; Nanoprobes, Inc., Stony Brook, NY) diluted 1:100 in dilution buffer. After washing with washing buffer, cells were postfixed for 15 min with 1% glutaraldehyde in PB, and gold labels were enhanced by a 6-min incubation with a silver developer (HQ silver, Nanoprobes) in the dark. Cells were postfixed again with 0.5% OsO_4 in PB for 90 min at 4 °C, stained with 4% uranyl acetate for 30 min at room temperature, and dehydrated by passage through a graded series of ethanol (50, 70, 90, and 100%). After embedding in Epon 812 (Nacalai Tesque), ultrathin sections (80 nm thickness) were cut with an LKB Ultratome (GE Healthcare), transferred to specimen grids coated with polyvinyl formal (Nissin EM Co., Tokyo, Japan), stained with uranyl acetate and lead citrate, and inspected under an electron microscope (JEM-1013EX, JEOL, Tokyo, Japan) (26).

RESULTS

EGFP-Kv12.2 Forms Functional Channels—We cloned the mouse *Kv12.2* gene (see "Experimental Procedures") and examined the activity of its product by recording whole-cell currents in transiently transfected CHO cells using the patch clamp technique. To identify transfected cells, EGFP was co-transfected with wild-type Kv12.2, but this approach did not allow us to reliably measure currents from EGFP-positive cell (data not shown). To improve the reproducibility of our measurements, we fused EGFP to the N terminus of Kv12.2. When cells were transfected with EGFP-Kv12.2, almost all EGFP-positive cells showed voltage-dependent transient outward currents and characteristic tail currents (Fig. 2), which were absent in mock-transfected cells. The currents were similar to those of untagged Kv12.2 channels which were previously reported (6, 8, 11). We, therefore, concluded that EGFP-Kv12.2 could be used for further characterization of the channel.

Electrophoretic Mobility of Recombinant EGFP-Kv12.2 and Native Kv12.2—To characterize the biochemical properties of Kv12.2, we performed an immunoblot analysis. We raised a polyclonal antibody against the very C terminus of mouse

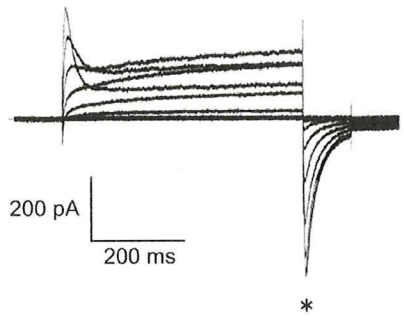

FIGURE 2. **Voltage-dependent current of EGFP-Kv12.2.** Representative currents were measured from CHO cells transfected with EGFP-Kv12.2. In this experiment, EGFP-Kv12.2 outward currents were elicited by voltage pulses from −80 to 80 mV for 500 ms from a holding potential of −80 mV. Tail currents were elicited by repolarizing the membrane to −120 mV at the end of the 500-ms pulses. The *asterisk* indicates the tail currents.

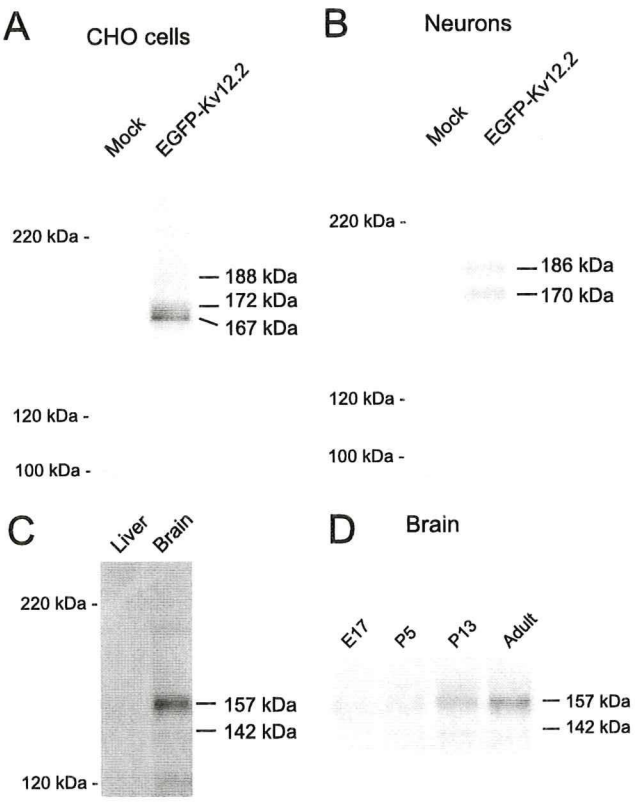

FIGURE 3. **Electrophoretic mobility of Kv12.2 channels.** Cell lysates or crude membranes were analyzed by SDS-PAGE and immunoblotting. *A*, *n*-dodecyl-β-D-maltopyranoside-solubilized lysates were prepared from CHO cells transfected with EGFP-Kv12.2 and mock-transfected cells. *B*, radioimmune precipitation assay buffer-solubilized lysates were prepared from hippocampal neurons transfected with EGFP-Kv12.2 and mock-transfected neurons. *C*, crude membranes were prepared from adult mouse brain and liver tissue at postnatal day 210. 20 μg of protein was loaded. *D*, equal amounts of crude membranes were analyzed at different developmental stages: embryonic day 17 (*E17*), postnatal day 5 (*P5*) and 13 (*P13*), and adult (P210). The molecular masses estimated from the protein standards are shown to the *right* of the *lanes*.

Kv12.2 (anti-Kv12.2(1081), see "Experimental Procedures") and used it to detect EGFP-Kv12.2 expressed in CHO cells. The anti-Kv12.2(1081) antibody recognized three prominent bands that were absent in mock-transfected CHO cells (Fig. 3*A*). The bands at molecular masses of 172 and 167 kDa were strong, whereas the band at the highest molecular mass (188 kDa) was faint. These molecular masses are bigger than the calculated molecular mass of the EGFP-Kv12.2 protein of 145 kDa, which includes 27 kDa for EGFP and the linker. The antibody did not cross-react with the closely related Kv12.3 channel expressed in CHO cells (supplemental Fig. S1), and another antibody (anti-Kv12.2(787), see "Experimental Procedures") produced a similar staining pattern on immunoblots (supplemental Fig. S1). We, therefore, conclude that the anti-Kv12.2(1081) antibody specifically recognizes Kv12.2 and that all three bands detected by anti-Kv12.2(1081) represent EGFP-Kv12.2.

Immunoblot analysis of EGFP-Kv12.2 expressed in cultured hippocampal neurons revealed only two bands (Fig. 3*B*). Their apparent molecular masses of 186 and 170 kDa suggested that they correspond to the upper (188 kDa) and middle (172 kDa) band seen in immunoblots of CHO cells expressing EGFP-Kv12.2.

When immunoblots of crude membranes from mouse brain were analyzed, the anti-Kv12.2(1081) antibody recognized two bands with apparent molecular masses of 157 and 142 kDa that were not detected in immunoblots of mouse liver membranes (Fig. 3*C*). These bands would correspond to the upper band (188 and 186 kDa) and the middle band (172 and 170 kDa) of EGFP-Kv12.2 expressed in heterologous systems (CHO cells and cultured neurons, respectively). The lower apparent molecular masses of the native channels are due to the lack of the 27-kDa EGFP. The faint bands at 200 and 120 kDa are likely due to nonspecific binding because these bands were not detected by the anti-Kv12.2(787) antibody. To examine temporal changes in the expression level and the biochemical properties of native Kv12.2 channels in the developing brain, equal amounts of membranes from whole brains of mice at four ages (embryonic day 17 (*E17*), postnatal day 5 (*P5*), P13, and P210 (adult)) were analyzed (Fig. 3*D*). The intensity of the predominant 157-kDa band increased steadily in the course of brain development, with the greatest change occurring between postnatal day 5 and P13. In contrast, the intensity of the 142-kDa band peaked at P13. The detection of multiple bands in these results suggested that Kv12.2 carries co- and/or post-translational modifications both *in vitro* and *in vivo*.

Kv12.2 Is N-Glycosylated—Among the various potential modifications of Kv12.2, we decided to focus on *N*-glycosylation because Kv12.2 contains three *N*-linked glycosylation consensus sequences in the unique S5-P loop (Fig. 1*B*). To investigate the *N*-glycosylation of Kv12.2, we performed immunoblot analysis of detergent-solubilized EGFP-Kv12.2 or crude mouse brain membrane preparations after removal of either high mannose-type oligosaccharides by Endo H or all types of oligosaccharides by PNGase F.

When EGFP-Kv12.2 expressed in CHO cells was treated with Endo H, the 172-kDa band disappeared, presumably shifting the protein to the 167-kDa band, which increased in intensity (Fig. 4*A*, *white arrowhead*). The 188-kDa band was not affected by Endo H treatment (Fig. 4*A*, *black arrow*). This result indicates that the 172-kDa band contains proteins carrying high mannose-type oligosaccharides. We will refer to this protein as the immature form of EGFP-Kv12.2. Treatment of recombinant EGFP-Kv12.2 with PNGase F, which can remove both high

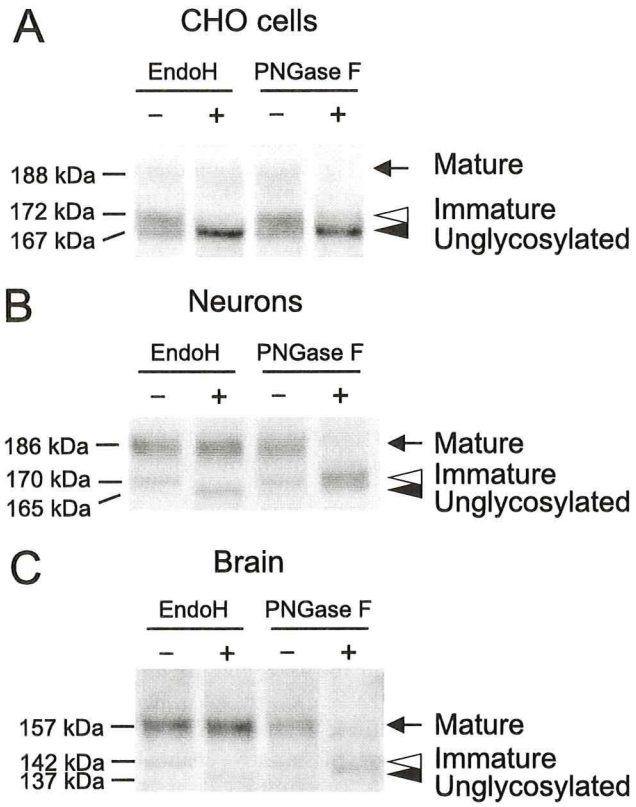

FIGURE 4. **Enzymatic deglycosylation of Kv12.2 channels.** Cell lysates or crude membranes were denatured and treated with endoglycosidases (Endo H or PNGase F) or buffer alone (−). *A*, lysate of CHO cells transfected with EGFP-Kv12.2 is shown. *B*, lysate of neurons transfected with EGFP-Kv12.2 is shown. *C*, crude membranes prepared from P13 mouse brain are shown. *Arrows* indicate the mature form of EGFP-Kv12.2 or native Kv12.2, which carries complex oligosaccharides. *Open arrowheads* indicate the immature form of EGFP-Kv12.2 or native Kv12.2, which carries high mannose oligosaccharides. *Filled arrowheads* indicate the unglycosylated or deglycosylated form of EGFP-Kv12.2 or native Kv12.2.

mannose and complex oligosaccharides, caused the 188-kDa band to completely disappear, and the intensity of the 172-kDa band was significantly reduced with a concomitant increase in the intensity of the 167-kDa band (Fig. 4*A*). This result suggests that the 188-kDa band contains proteins carrying complex oligosaccharides, and we will refer to this protein as the mature form of EGFP-Kv12.2. The 167-kDa band did not shift even after PNGase F treatment (Fig. 4*A*, *black arrowhead*), indicating that it represents unglycosylated EGFP-Kv12.2. These results demonstrate that EGFP-Kv12.2 expressed in CHO cells is *N*-glycosylated.

In primary cultured neurons, similar band shifts were observed when detergent-solubilized EGFP-Kv12.2 was treated with endoglycosidases (Fig. 4*B*). The experiments revealed that in cultured neurons the 186-kDa band represents the mature channel carrying complex oligosaccharides, and the 170-kDa band represents the immature channel carrying high mannose oligosaccharides. The lack of a 165-kDa band, which would correspond to unglycosylated EGFP-Kv12.2 (Fig. 4*B*, *black arrowhead*) indicates that only a negligible fraction of EGFP-Kv12.2 in cultured neurons exists in an unglycosylated form.

The 157-kDa band seen with native Kv12.2 from mouse brain was resistant to Endo H but sensitive to PNGase F, whereas the 142-kDa band was sensitive to both enzymes (Fig. 4*C*). Like recombinant EGFP-Kv12.2 in cultured neurons, native Kv12.2 appears to exist in the mouse brain in a mature form carrying complex oligosaccharides (157-kDa band) and an immature form carrying high-mannose oligosaccharides (142-kDa band) with an undetectable level of unglycosylated protein.

From these results we conclude that Kv12.2 is *N*-glycosylated both *in vivo* as well as in heterologous expression systems. The bands representing deglycosylated Kv12.2 after PNGase F treatment were diffuse (Fig. 4). This may be due to α1,3-linked fucose residues in the sugar chains, which render *N*-glycans resistant to cleavage by PNGase F (27). It is also possible that mature Kv12.2 undergoes another post-translational modification that affects the electrophoretic mobility. The ratio of mature to immature and unglycosylated Kv12.2 was higher in mouse brain and cultured neurons than in CHO cells. The inefficient maturation of EGFP-Kv12.2 in CHO cells was not due to the fused EGFP, because the analysis of Kv12.2 without EGFP expressed in CHO cells yielded similar results (supplemental Fig. S2). The observed molecular masses of deglycosylated EGFP-Kv12.2 and deglycosylated Kv12.2 from mouse brain are bigger than the calculated molecular mass of the core protein by ~20 kDa. The difference between the apparent and calculated molecular masses may indicate that Kv12.2 carries post-translational modifications other than *N*-linked glycosylation or may be due to a slightly aberrant mobility of Kv12.2 in SDS-PAGE gels, which is not uncommon for membrane proteins.

Glycosylation Is Not Required for Kv12.2 Channel Function—*N*-Linked glycosylation may play an important role in channel function itself and/or in defining channel characteristics because the *N*-glycosylation sites of Kv12.2 are located in the long extracellular S5-P loop near the pore region (Fig. 1*A*, *right panel*). To determine whether glycosylation affects channel function itself, we measured the tail currents of CHO cells expressing wild-type EGFP-Kv12.2 after enzymatic removal of the sugar chains with PNGase F. Because only channels in the plasma membrane are measured, this experimental design eliminated any potential effects related to protein trafficking. We first treated live CHO cells expressing EGFP-Kv12.2 with increasing concentrations of PNGase F and evaluated its efficiency (Fig. 5*A*). Although PNGase F could affect high mannose-type oligosaccharides of detergent-solubilized EGFP-Kv12.2 (Fig. 4*A*), treatment of the cells with 500 units/ml PNGase F only affected complex sugar chains of EGFP-Kv12.2 (Fig. 5*A*, *arrow*), and even higher enzyme concentrations did not remove high mannose-type oligosaccharides (Fig. 5*A*, *white arrowhead*). This result shows that PNGase F can remove sugar chains of EGFP-Kv12.2 on live cells and suggests that only the mature form of Kv12.2 carrying complex oligosaccharides is expressed on the cell surface. When we measured the EGFP-Kv12.2 tail currents after removal of the sugar chains by 1000 units/ml PNGase F, the current amplitude was not significantly reduced as compared with the controls (Fig. 5*B*). This result indicates that sugar chains are not necessary for the Kv12.2 channel function itself.

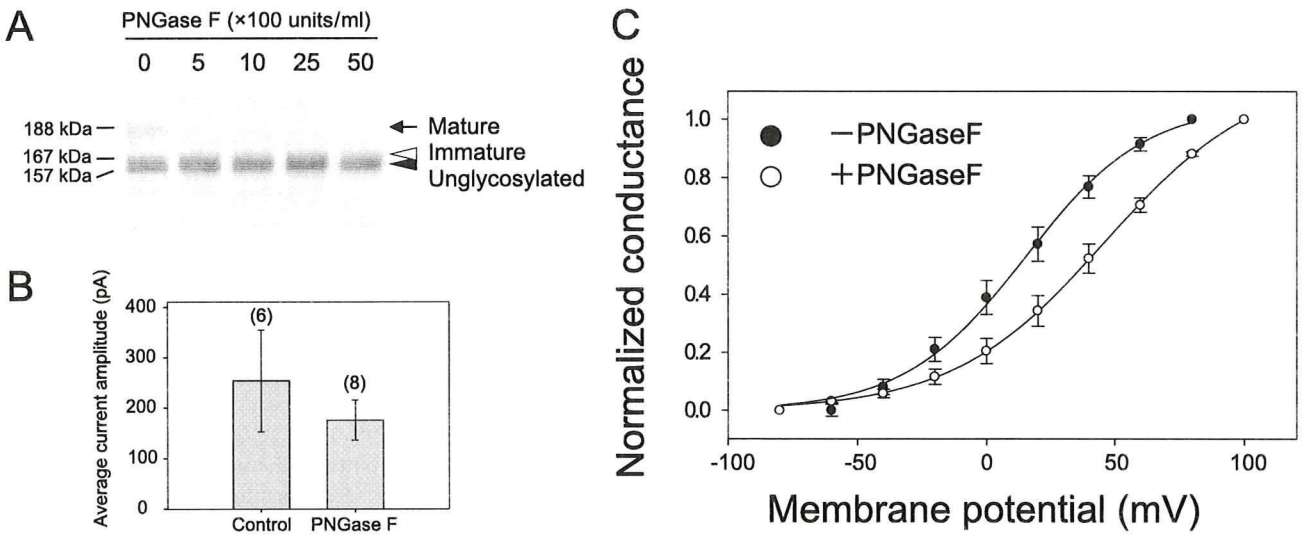

FIGURE 5. **Effect of glycosylation on the current amplitude and steady-state activation of EGFP-Kv12.2 expressed in CHO cells.** *A*, an immunoblot of lysate from CHO cells transfected with EGFP-Kv12.2 and treated with PNGase F is shown. CHO cells transfected with wild-type EGFP-Kv12.2 were incubated at 37 °C for 1 h with 0, 500, 1000, 2500, or 5000 units/ml PNGase F in PBS supplemented with 1 mM $MgCl_2$ and 1 mM $CaCl_2$. The *arrow* indicates the mature form of EGFP-Kv12.2, the *open arrowhead* indicates the immature form, and the *filled arrowhead* indicates unglycosylated EGFP-Kv12.2. *B* and *C*, CHO cells transfected with EGFP-Kv12.2 were treated with 1000 units/ml or without PNGase F (*filled circles* or *open circles* in Fig. 5*C*, respectively). *B*, shown are average current amplitudes of the treated cell. The *numbers* in *parentheses* indicate the number of experiments. *C*, the activation curve obtained using the tail-current protocol is shown. For PNGase F-treated cells, the half-maximal activation voltage ($V_{1/2}$) was 46.5 ± 1.3 mV, and the slope factor (*k*) was 29.9 ± 0.7 mV ($n = 5$, *open circles*); for control cells $V_{1/2}$ was 15.1 ± 2.5 mV, and *k* was 23.7 ± 1.7 mV ($n = 5$, *filled circles*). *Error bars* correspond to the S.E. of the mean.

Deglycosylation Causes a Depolarizing Shift in the Voltage-dependent Activation of Kv12.2—We next focused on the role of *N*-glycosylation in the channel characteristics. To examine the effect of glycosylation on the voltage dependence of Kv12.2, we determined the steady-state activation of EGFP-Kv12.2 before and after PNGase F treatment of live CHO cells expressing EGFP-Kv12.2 (Fig. 5*C*). The steady-state activation was evaluated according to an established tail-current protocol (see the legend to Fig. 5*C* and Refs. 6, 8, and 11 for details). The membrane potential was stepped from a holding potential to conditioning potentials between −80 and 80 mV. Tail currents were elicited during a subsequent repolarizing step, where the inactivated channels recover quickly to the open state as in Fig. 2. Therefore, the tail current reflects the number of open channels at a conditioning potential. The normalized peak amplitudes of the tail currents were plotted against the conditioning potentials (Fig. 5*C*). The half-maximal activation voltage of glycosylated EGFP-Kv12.2 was 15.1 ± 2.5 mV ($n = 5$, Fig. 5*C*, *filled circles*), but that of deglycosylated EGFP-Kv12.2 was 46.5 ± 1.3 mV ($n = 5$, Fig. 5*C*, *open circles*). Thus, removal of sugar chains by PNGase F treatment caused a depolarizing shift in the voltage-dependent activation by ~30 mV.

The Deglycosylation-induced Shift in Voltage-dependent Activation Is Not Due to the Loss of Sialic Acid Residues—Previous studies have reported that *N*-glycosylation can affect voltage-dependent activation of potassium channels and sodium channels via negatively charged sialic acids. The removal of sialic acids causes a depolarizing shift in the activation voltage by ~10–20 mV (28–31). The effect of sialic acids on the channels was attributed to the electrostatic influence of these negatively charged residues, which alters the effective electric field detected by the voltage sensors of the channels. We speculated that the effect of *N*-glycans on Kv12.2 (Fig. 5*C*) is also caused by sialic acid residues in the sugar chains. To examine this possibility, we treated cells expressing wild-type EGFP-Kv12.2 with neuraminidase (sialidase) and analyzed them by immunoblotting and patch clamp recording. Immunoblots demonstrated that neuraminidase caused a band shift of 4 kDa (Fig. 6*A*). This result shows that EGFP-Kv12.2 expressed in CHO cells carries sialic acids and that these can be removed by neuraminidase treatment of live CHO cells. The steady-state activation of the desialylated EGFP-Kv12.2 channel was measured by the same tail-current protocol used in Fig. 5*C* (Fig. 6*B*). The half-maximal activation voltage after neuraminidase treatment was 12.3 ± 2.8 mV ($n = 4$, Fig. 6*B*, *open circles*), similar to that measured with untreated cells (Fig. 6*B*, *filled circles*, same data as in Fig. 5*C*). This result suggests that the deglycosylation-induced shift in the steady-state activation curve of the EGFP-Kv12.2 channel is due to a mechanism that is different from the electrostatic influence of the sialic acid residues.

Unglycosylated Kv12.2 Is Not Expressed on the Cell Surface—We next focused on the trafficking of unglycosylated channels to know whether unglycosylated channels, which have a different voltage dependence from glycosylated channels (Fig. 5*C*), are utilized *in vivo*. To address this issue we analyzed CHO cells expressing EGFP-Kv12.2 that were treated with tunicamycin, which inhibits *N*-linked glycosylation. Immunoblots revealed a single band of 167 kDa, corresponding to the size of EGFP-Kv12.2 after PNGase F treatment (Fig. 7*A*). This finding corroborated our conclusion that the 188- and 172-kDa bands correspond to glycosylated protein, and the 167-kDa bands correspond to unglycosylated protein and confirmed that tunicamycin effectively inhibits *N*-linked glycosylation in this system.

To study the expression of unglycosylated Kv12.2 channels on the cell surface, we performed patch clamp studies on trans-

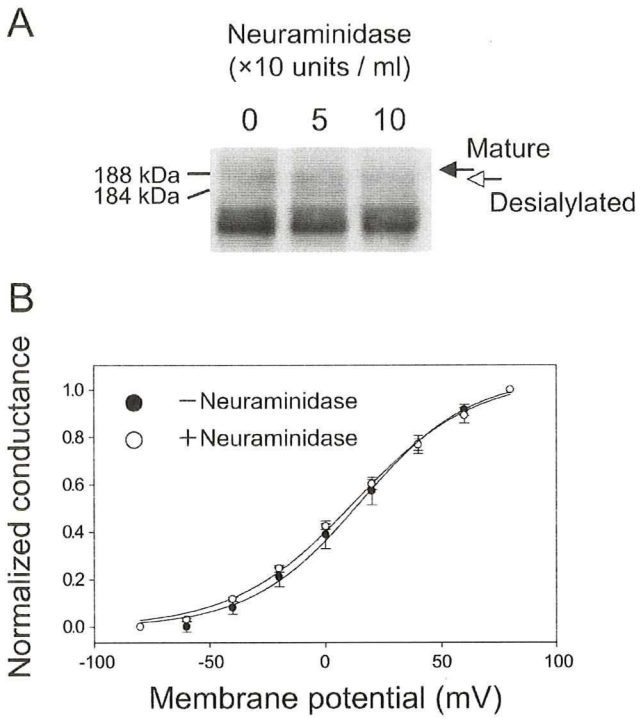

FIGURE 6. **Effect of sialic acid residues on the steady-state activation of EGFP-Kv12.2 expressed in CHO cells.** *A*, shown is an immunoblot of lysate from EGFP-Kv12.2-transfected cells after neuraminidase treatment. Cells transfected with wild-type EGFP-Kv12.2 were treated as in Fig. 5*A*, except that three different concentrations of neuraminidase were used in this experiment: 0, 50, or 100 units/ml. The *black arrow* indicates the fully glycosylated form of EGFP-Kv12.2, and the *white arrow* indicates the desialylated EGFP-Kv12.2 channel. *B*, shown is an activation curve of untreated (*filled circles*) and neuraminidase-treated (*open circles*) EGFP-Kv12.2. To remove sialic acid residues, 50 units/ml neuraminidase were added to live CHO cells transfected with EGFP-Kv12.2. The activation curves were obtained following the same tail-current protocol used in Fig. 5*C*. *Error bars* correspond to the S.E. For neuraminidase-treated cells, $V_{1/2}$ was 12.3 ± 2.8 mV, and the slope factor was 25.8 ± 1.8 mV (n = 4); for control cells, the values are the same as those in Fig. 5*C*.

fected CHO cells after tunicamycin treatment. If unglycosylated channels are expressed on the cell surface, tail currents would be observable because Kv12.2 channels lacking sugar chains are functional (Fig. 5*B*). Fig. 7*B* shows representative tail currents measured from EGFP-Kv12.2-transfected cells after treatment with tunicamycin or DMSO. Treatment of the cells with tunicamycin resulted in the loss of Kv12.2 current. Quantitative analysis of the data showed that tunicamycin treatment caused a dramatic reduction in the average current amplitude of EGFP-Kv12.2 (Fig. 7*C*). This result implies that unglycosylated Kv12.2 is not trafficked to the cell surface.

Expression of Kv12.2 on the Cell Surface Requires at Least One of the Three Glycosylation Sites to Carry a Sugar Chain—Kv12.2 has three consensus sequences for *N*-linked glycosylation at asparagines 421, 428, and 447 (Fig. 1*B*). Tunicamycin treatment inhibits the glycosylation of all three sites. To investigate how the number and position of *N*-glycosylation at these three sites affect maturation and cell surface expression of Kv12.2, we used site-directed mutagenesis to generate glutamine substitution mutants, specifically the three single mutants N421Q, N428Q, and N447Q (designated as EGFP-Kv12.2 QNN, NQN, and NNQ), the three double mutants N421Q,N428Q, N421Q,N447Q, and N428Q,N447 (designated as EGFP-Kv12.2 QQN, QNQ, and NQQ), and the triple mutant N421Q,N428Q,N447Q (designated as EGFP-Kv12.2 QQQ).

Immunoblots of the single mutants EGFP-Kv12.2 QNN, NQN, and NNQ showed three bands corresponding to the mature, immature, and unglycosylated form of the wild-type channel (Fig. 8*A*). In contrast, immunoblots of the double mutants EGFP-Kv12.2 QQN, QNQ, and NQQ showed only the bands representing the immature and unglycosylated form, but the mature form could no longer be detected (Fig. 8*A*). This result demonstrates that all three sites are potentially glycosylated and suggests that the maturation of the double mutants was less efficient than that of the wild type and single mutants. The triple mutant EGFP-Kv12.2 QQQ showed only one sharp band with the same mobility as the wild-type protein treated with PNGase F (Fig. 8*A*). Furthermore, PNGase F treatment had no effect on the electrophoretic mobility of the triple mutant (data not shown). These results suggest that *N*-linked glycosylation at sites Asn-421, Asn-428, and Asn-447 account for all the *N*-linked oligosaccharides on the Kv12.2 channel.

The function of the substitution mutants was analyzed by measuring their tail currents (Fig. 8*B*). CHO cells transfected with single mutants showed average current amplitudes similar to cells transfected with wild-type EGFP-Kv12.2. The average current amplitude was slightly reduced in cells transfected with double mutants and significantly reduced in cells transfected with the triple mutant (Fig. 8*B*). This result indicates that expression of Kv12.2 on the cell surface requires at least one of the three glycosylation sites to carry a sugar chain irrespective of their positions.

Intracellular Distribution and Surface Expression of Unglycosylated Kv12.2—The lack of current seen in CHO cells expressing wild-type EGFP-Kv12.2 after tunicamycin treatment (Fig. 7, *B* and *C*) and cells expressing the EGFP-Kv12.2 QQQ triple mutant (Fig. 8*B*) must be due to inefficient trafficking of the channels to the cell surface, because removal of sugar chains did not diminish the current amplitude (Fig. 5*B*). To further corroborate our conclusion, we used fluorescence microscopy to analyze the subcellular localization of the channels. In CHO cells expressing EGFP-Kv12.2 wild type and QQQ triple mutant, most of the signal localized to intracellular or perinuclear compartments, co-localizing mainly with endoplasmic reticulum marker (supplemental Fig. S3). To better detect the signal on the cell surface, we then used confocal microscopy, which revealed the EGFP signal at the cell membrane in cells expressing wild-type EGFP-Kv12.2 (Fig. 9, *A*, *left panel* and *B*, *arrows*). In contrast, no EGFP signal was seen at the cell surface in cells expressing the triple mutant (Fig. 9*A*, *right panel*). This subcellular distribution was further analyzed by immunoelectron microscopy with anti-EGFP antibodies, which confirmed the plasma membrane localization of wild-type EGFP-Kv12.2 (Fig. 9, *C*, *left panel* and *D*, *arrows*) but not of the triple mutant (Fig. 9*C*, *right panel*). We, therefore, conclude that *N*-glycosylation is necessary for intracellular trafficking of the Kv12.2 channel to the cell surface.

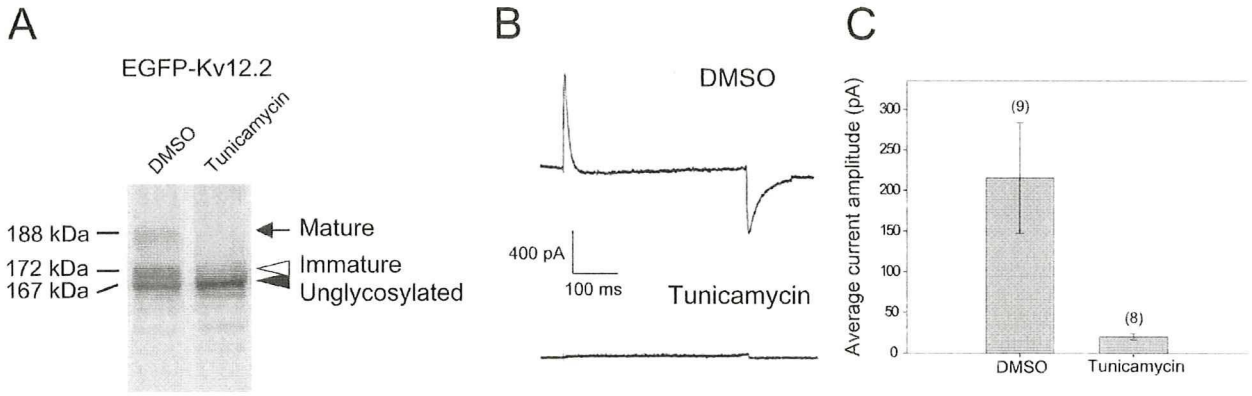

FIGURE 7. **Effects of tunicamycin treatment on the glycosylation and function of Kv12.2 in CHO cells.** 8–10 h after transfection with EGFP-Kv12.2, CHO cells were treated with 5 μg/ml tunicamycin or DMSO as control. *A*, shown is an immunoblot of lysates from tunicamycin- and DMSO-treated CHO cells. The *arrow* indicates the mature form of EGFP-Kv12.2, the *open arrowhead* indicates the immature form, and the *filled arrowhead* indicates unglycosylated EGFP-Kv12.2. *B*, representative currents recorded from tunicamycin- and DMSO-treated CHO cells are shown. Tail current was elicited by a voltage step at −100 mV after a conditioning pulse of 120 mV for 500 ms. *C*, shown are average amplitudes of peak tail currents measured from tunicamycin- and DMSO-treated CHO cells. *Error bars* correspond to the S.E., and the *numbers* in *parentheses* indicate the number of cells measured.

DISCUSSION

In this study we demonstrate that *N*-linked glycosylation plays two important roles in Kv12.2. 1) *N*-linked glycans regulate the voltage-dependent activation of Kv12.2 through a mechanism that is independent of the presence of negatively charged sialic acid residues in the sugar chains. 2) Although the position is not crucial, at least one of the three glycosylation sites has to carry a sugar chain for Kv12.2 to be trafficked to the cell surface. In addition, our results provide evidence that Kv12.2 exists mostly in a glycosylated form in the mouse brain. These results suggest that *N*-glycosylated Kv12.2 is likely to function *in vivo*, whereas unglycosylated Kv12.2, which has different channel properties, is unlikely to have any functional significance.

We showed that removal of *N*-glycans results in a depolarizing shift in the voltage-dependent activation of Kv12.2 by ~30 mV (Fig. 5*C*). A similar effect of sugar chains, especially of negatively charged sialic acid residues, has been reported for voltage-dependent potassium channels (Kv) and sodium channels (Nav) (19, 23, 28, 30). Enzymatic removal of the entire sugar chain or only the sialic acid residues from purified, transfected, or endogenous Kv and Nav channels shifted gating in the depolarized direction (23, 31, 32). Moreover, when some Kv and Nav α-subunit isoforms were expressed in the Lec2 mutant CHO cell line, which exhibits reduced sialylation, the channels opened at more depolarized potentials (19, 28, 29, 31). Reduced sialylation of these channels is thought to change their external surface charge, causing a shift in their activation curve by 10~20 mV. Unexpectedly, in the case of Kv12.2, removal of sialic acids did not affect the steady-state activation curve (Fig. 6*B*). It is possible that Kv12.2 is modified by sialic acids that are resistant to neuraminidase added to live cells. Alternatively, the observed shift may be caused by a novel mechanism that is independent of the sialic acid residues. Possibly, the sugar chains directly interact with the channel itself and regulate its function. It has been reported that the S5-P loop in members of the EAG family contains an amphipathic α-helix, which interacts with the voltage sensor and contributes to the different inactivation characteristics of the channels (33–35). This suggests that the sugar chains in the long S5-P loop could also interact with a part of the channel itself such as the voltage sensor. The recent structure of a Kv1.2–2.1 chimera channel together with its β-subunit provided important insights into the gating of voltage-dependent channels, but it did not provide structural information on the sugar chains (36). Ideally, to understand channel gating under the most native conditions, structural information should be obtained for voltage-dependent channels carrying their native sugar chains. However, the heterogeneous and flexible nature of sugar chains often prevent the growth of three-dimensional crystals and/or are too disordered in crystals to be resolved in the resulting density map.

Our results from the inhibition of *N*-glycosylation by tunicamycin (Fig. 7) and the analysis of glutamine mutants (Figs. 8 and 9) showed that unglycosylated Kv12.2 channels are not trafficked to the cell surface in CHO cells. The Eag (Kv10.1) channel and the HERG (Kv11.1) channel, other members of the EAG family (Kv10.x ~ Kv12.x, Fig. 1*B*), also require glycosylation for their proper cell surface trafficking (18, 20, 25). In the Kv10.1 channel the two glycosylation sites in the S5-P loop appear not to be equivalent, as it has been shown that proper complex glycosylation of at one of the two sites is crucial for proper trafficking of the channel and its functional properties (18). In contrast, the three sites of Kv12.2 appear to be equivalent at least for channel trafficking because all double mutants showed current amplitudes only slightly lower than that of the wild-type EGFP-Kv12.2 (Fig. 9*B*). The recognition mechanism of sugar chains or the structure of the S5-P loop may, thus, vary, even between members of the EAG family.

Here we presented the first biochemical data for *N*-glycosylation of Kv12.2. In the adult mouse Kv12.2 protein is expressed in the brain but not in the liver (Fig. 3*C*). This result is consistent with the brain-specific expression of its mRNA (6–8). The level of mature Kv12.2 protein increases with development (Fig. 3*D*). This result is also consistent with the up-regulation of Kv12.2 mRNA in the rat brain (6). A similar increase in protein level with development has been reported for other potassium channels, including

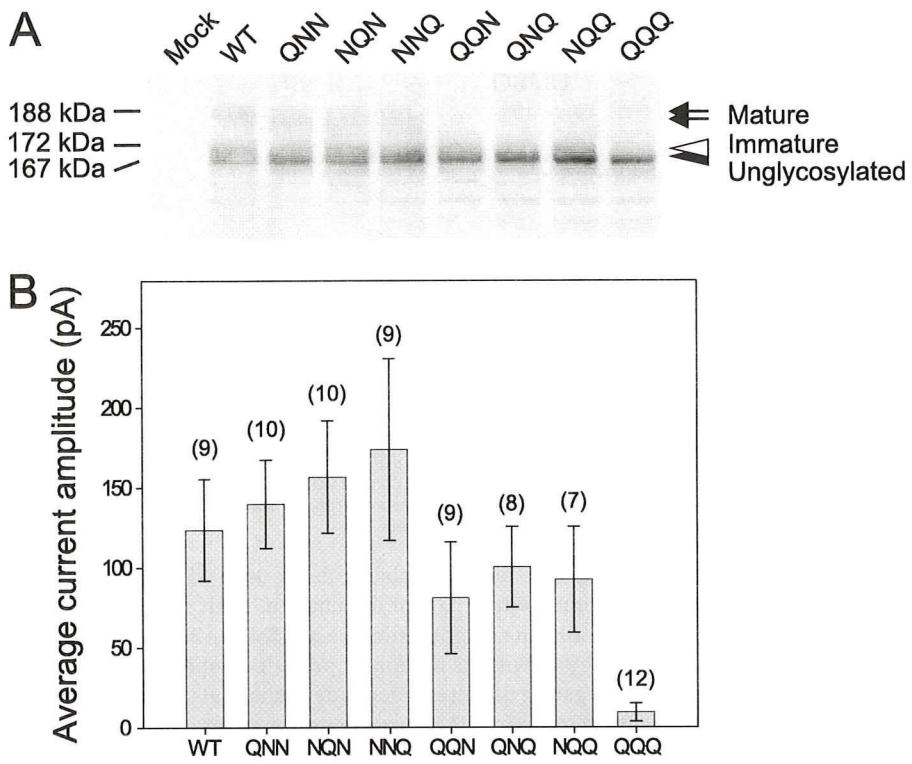

FIGURE 8. **Biochemical and electrophysiological analyses of Kv12.2 substitution mutants.** CHO cells were transfected with mutants in which the asparagine residues in the three glycosylation sites were substituted with glutamine residues (see "Results" for details). *A*, shown is an immunoblot of wild-type (*WT*) EGFP-Kv12.2 and the substitution mutants. The *arrow* indicates the mature form of EGFP-Kv12.2, the *open arrowhead* indicates the immature form, and the *filled arrowhead* indicates unglycosylated EGFP-Kv12.2. *B*, average current amplitudes are shown of the peak tail currents measured from the transfected CHO cells as in Fig. 5*B*. *Error bars* correspond to the S.E., and the *numbers* in *parentheses* indicate the number of cells measured.

Kv1.4, Kv1.5, Kv2.1, and Kv2.2 (37). This increase in the expression of Kv12.2 may be partly due to the postnatal increase in synaptogenesis and suggests that Kv12.2 is involved in the excitability of neurons. In our experiments the unglycosylated form of Kv12.2 was not observed in the mouse brain. This finding together with the fact that unglycosylated EGFP-Kv12.2 was not trafficked to the cell surface in CHO cells suggests that unglycosylated Kv12.2 is not utilized *in vivo*. Unlike in mouse brain and in cultured neurons, the unglycosylated and immature forms are predominant in the non-neuronal CHO cells even for the wild-type channels. This result suggests that Kv12.2 does not mature efficiently when transiently expressed in non-neuronal cells like CHO cells. Because the final maturation steps of sugar chains occur in the Golgi apparatus, the preponderance of immature and unglycosylated channels suggested that the channel is retained in the endoplasmic reticulum (13). Immunofluorescence microscopy of CHO cells expressing EGFP-Kv12.2 supported this notion, because the majority of the signal co-localized with endoplasmic reticulum markers (supplemental Fig. S3). These results indicate that Kv12.2 may require some factors for efficient maturation and/or efficient trafficking and these factors might only be present in neuronal cells but are lacking in non-neuronal cells, such as CHO cells. Certain channels are known to require auxiliary molecules, such as β-subunits, for proper folding and/or trafficking (38, 39). For example, Kvβ2 promotes co-translational *N*-linked glycosylation of the nascent Kv1.2 polypeptide and increases the efficiency of its cell surface expression (40). Kv12.2 may, thus, also need a β-subunit for efficient glycosylation and cell surface expression. Another possibility is that, as a recent study showed using *Xenopus* oocytes (41), intrinsic KCNE1 and KCNE3 may down-regulate the cell surface expression of Kv12.2 in CHO cells.

Finally, we discuss why Kv12.2 features an unusually long S5-P loop and has as many as three glycosylation sites. These structural features are unique to mammalian Kv12.2. The fruit fly ortholog Elk, the zebrafish ortholog Elk1, and the mammalian paralogs Kv12.1 and Kv12.3 lack both of them (Fig. 1*B*), whereas they are conserved in all known mammalian Kv12.2 channels. This suggests that all three *N*-glycans would play important roles in the regulation of the mammalian Kv12.2 channel. One *N*-glycosylation site is sufficient for trafficking (Fig. 8*B*), and the additional two *N*-glycans are, therefore, likely to have some other roles. As we have shown here, one role is to regulate the steady-state activation of Kv12.2. Further analysis is required to elucidate how the number and/or position of the sugar chains affect the functions of Kv12.2. *N*-Glycosylation of these three sites may also be involved in the folding and/or stability of the channel. Many membrane proteins are known to require *N*-glycosylation for efficient folding and/or stability (42). These *N*-glycans are recognized by molecular chaperons such as calnexin and calreticulin (43). It has been reported that the number of *N*-glycans correlates with the affinity of these chaperons and the folding rate (44, 45). Here, we observed a small reduction in the current amplitude (Fig. 8*B*) and inefficient maturation of double mutants (Fig. 8*A*) that have only one glycosylation site (Fig. 1*B*) compared with the wild-type protein and the single mutants. This observation may suggest that the three glycosylation sites are required for proper folding by mediating interactions with molecular chaperons. The three glycosylation sites of Kv12.2 would, thus, serve several distinct functions. The glycosylation sites are located in an extended region of the S5-P loop. The S5-P loop may have to be long to properly display the three glycosylation sites, in particular because efficient *N*-glycosylation typically only occurs on sites that are 10 amino acids removed from a transmembrane region (46, 47). It is also pos-

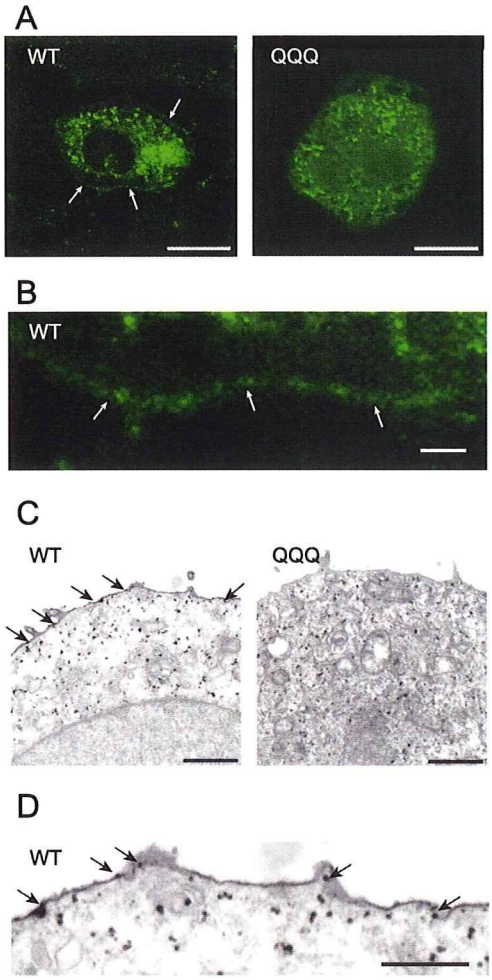

FIGURE 9. **Intracellular distribution of wild-type EGFP-Kv12.2 and QQQ mutant channels in CHO cells.** *A*, shown are confocal microscope images of CHO cells transfected with wild-type (*WT*) EGFP-Kv12.2 (*left panel*) or the QQQ mutant (*right panel*). *White arrows* point to the EGFP signals on the cell surface of a CHO cell expressing wild-type EGFP-Kv12.2. *Scale bars* represent 10 μm. *B*, shown is a higher magnification image of the cell membrane of the cell expressing wild-type EGFP-Kv12.2 shown in *panel A*. The *scale bar* represents 1 μm. *C*, electron microscope images are shown of CHO cells transfected with wild-type EGFP-Kv12.2 (*left panel*) or the QQQ mutant (*right panel*). The cells were labeled with gold-conjugated antibodies against EGFP. *Black arrows* point to immunogold localized on the cell surface. *Scale bars* represent 1 μm. *D*, shown is a higher magnification image of the cell membrane of the cells expressing wild-type EGFP-Kv12.2 shown in *panel C*. *Scale bar* represents 0.5 μm.

sible that the long S5-P loop itself has a specific, yet to be identified function.

Acknowledgments—We thank Drs. Hitoshi Niwa and Masatoshi Takeichi (RIKEN, Center for Developmental Biology) for kindly providing pCA plasmid and Drs. Christoph Gerle and Tomoko Doi for valuable discussions. We are grateful to Dr. Thomas Walz for critical reading of the manuscript.

REFERENCES

1. Hille, B. (2001) *Ion Channels of Excitable Membranes*, 3rd Ed., Sinauer Associates Sunderland, MA
2. Coetzee, W. A., Amarillo, Y., Chiu, J., Chow, A., Lau, D., McCormack, T., Moreno, H., Nadal, M. S., Ozaita, A., Pountney, D., Saganich, M., Vega-Saenz de Miera, E., and Rudy, B. (1999) *Ann. N.Y. Acad. Sci.* **868,** 233–285
3. Yu, F. H., and Catterall, W. A. (2004) *Sci. STKE 2004*, re15
4. Ganetzky, B., Robertson, G. A., Wilson, G. F., Trudeau, M. C., and Titus, S. A. (1999) *Ann. N.Y. Acad. Sci.* **868,** 356–369
5. Bauer, C. K., and Schwarz, J. R. (2001) *J. Membr. Biol.* **182,** 1–15
6. Engeland, B., Neu, A., Ludwig, J., Roeper, J., and Pongs, O. (1998) *J. Physiol.* **513,** 647–654
7. Miyake, A., Mochizuki, S., Yokoi, H., Kohda, M., and Furuichi, K. (1999) *J. Biol. Chem.* **274,** 25018–25025
8. Trudeau, M. C., Titus, S. A., Branchaw, J. L., Ganetzky, B., and Robertson, G. A. (1999) *J. Neurosci.* **19,** 2906–2918
9. Zou, A., Lin, Z., Humble, M., Creech, C. D., Wagoner, P. K., Krafte, D., Jegla, T. J., and Wickenden, A. D. (2003) *Am. J. Physiol. Cell Physiol.* **285,** C1356–C1366
10. Gutman, G. A., Chandy, K. G., Grissmer, S., Lazdunski, M., McKinnon, D., Pardo, L. A., Robertson, G. A., Rudy, B., Sanguinetti, M. C., Stühmer, W., and Wang, X. (2005) *Pharmacol. Rev.* **57,** 473–508
11. Becchetti, A., De Fusco, M., Crociani, O., Cherubini, A., Restano-Cassulini, R., Lecchi, M., Masi, A., Arcangeli, A., Casari, G., and Wanke, E. (2002) *Eur. J. Neurosci.* **16,** 415–428
12. Grosso, S., Pucci, L., Farnetani, M., Di Bartolo, R. M., Galimberti, D., Mostardini, R., Anichini, C., Balestri, M., Morgese, G., and Balestri, P. (2004) *J. Child Neurol.* **19,** 604–608
13. Helenius, A., and Aebi, M. (2001) *Science* **291,** 2364–2369
14. Burda, P., and Aebi, M. (1999) *Biochim. Biophys. Acta* **1426,** 239–257
15. Watanabe, I., Zhu, J., Sutachan, J. J., Gottschalk, A., Recio-Pinto, E., and Thornhill, W. B. (2007) *Brain Res.* **1144,** 1–18
16. Watanabe, I., Zhu, J., Recio-Pinto, E., and Thornhill, W. B. (2004) *J. Biol. Chem.* **279,** 8879–8885
17. Brooks, N. L., Corey, M. J., and Schwalbe, R. A. (2006) *FEBS J.* **273,** 3287–3300
18. Napp, J., Monje, F., Stühmer, W., and Pardo, L. A. (2005) *J. Biol. Chem.* **280,** 29506–29512
19. Watanabe, I., Wang, H. G., Sutachan, J. J., Zhu, J., Recio-Pinto, E., and Thornhill, W. B. (2003) *J. Physiol.* **550,** 51–66
20. Petrecca, K., Atanasiu, R., Akhavan, A., and Shrier, A. (1999) *J. Physiol.* **515,** 41–48
21. Misonou, H., and Trimmer, J. S. (2004) *CRC Crit. Rev. Biochem. Mol. Biol.* **39,** 125–145
22. Vacher, H., Mohapatra, D. P., and Trimmer, J. S. (2008) *Physiol. Rev.* **88,** 1407–1447
23. Thornhill, W. B., Wu, M. B., Jiang, X., Wu, X., Morgan, P. T., and Margiotta, J. F. (1996) *J. Biol. Chem.* **271,** 19093–19098
24. Sutachan, J. J., Watanabe, I., Zhu, J., Gottschalk, A., Recio-Pinto, E., and Thornhill, W. B. (2005) *Brain Res.* **1058,** 30–43
25. Gong, Q., Anderson, C. L., January, C. T., and Zhou, Z. (2002) *Am. J. Physiol. Heart Circ. Physiol.* **283,** H77–H84
26. Mizoguchi, A., Nakanishi, H., Kimura, K., Matsubara, K., Ozaki-Kuroda, K., Katata, T., Honda, T., Kiyohara, Y., Heo, K., Higashi, M., Tsutsumi, T., Sonoda, S., Ide, C., and Takai, Y. (2002) *J. Cell Biol.* **156,** 555–565
27. Tretter, V., Altmann, F., and März, L. (1991) *Eur. J. Biochem.* **199,** 647–652
28. Bennett, E., Urcan, M. S., Tinkle, S. S., Koszowski, A. G., and Levinson, S. R. (1997) *J. Gen. Physiol.* **109,** 327–343
29. Bennett, E. S. (2002) *J. Physiol.* **538,** 675–690
30. Johnson, D., and Bennett, E. S. (2008) *Pflugers Arch.* **456,** 393–405
31. Ufret-Vincenty, C. A., Baro, D. J., and Santana, L. F. (2001) *Am. J. Physiol. Cell Physiol.* **281,** C464–C474
32. Recio-Pinto, E., Thornhill, W. B., Duch, D. S., Levinson, S. R., and Urban, B. W. (1990) *Neuron* **5,** 675–684
33. Liu, J., Zhang, M., Jiang, M., and Tseng, G. N. (2002) *J. Gen. Physiol.* **120,** 723–737
34. Dun, W., Jiang, M., and Tseng, G. N. (1999) *Pflugers Arch.* **439,** 141–149
35. Jiang, M., Zhang, M., Maslennikov, I. V., Liu, J., Wu, D. M., Korolkova, Y. V., Arseniev, A. S., Grishin, E. V., and Tseng, G. N. (2005) *J. Physiol.* **569,** 75–89
36. Long, S. B., Tao, X., Campbell, E. B., and MacKinnon, R. (2007) *Nature*

450, 376–382
37. Maletic-Savatic, M., Lenn, N. J., and Trimmer, J. S. (1995) *J. Neurosci.* **15,** 3840–3851
38. Pongs, O., Leicher, T., Berger, M., Roeper, J., Bähring, R., Wray, D., Giese, K. P., Silva, A. J., and Storm, J. F. (1999) *Ann. N.Y. Acad. Sci.* **868,** 344–355
39. Torres, Y. P., Morera, F. J., Carvacho, I., and Latorre, R. (2007) *J. Biol. Chem.* **282,** 24485–24489
40. Shi, G., Nakahira, K., Hammond, S., Rhodes, K. J., Schechter, L. E., and Trimmer, J. S. (1996) *Neuron* **16,** 843–852
41. Clancy, S. M., Chen, B., Bertaso, F., Mamet, J., and Jegla, T. (2009) *PLoS ONE* **4,** e6330
42. Varki, A. (1993) *Glycobiology* **3,** 97–130
43. Helenius, A., and Aebi, M. (2004) *Ann. Rev. Biochem.* **73,** 1019–1049
44. Vanoni, O., Paganetti, P., and Molinari, M. (2008) *Mol. Biol., Cell* **19,** 4086–4098
45. Hebert, D. N., Zhang, J. X., Chen, W., Foellmer, B., and Helenius, A. (1997) *J. Cell Biol.* **139,** 613–623
46. Zhu, J., Recio-Pinto, E., Hartwig, T., Sellers, W., Yan, J., and Thornhill, W. B. (2009) *Brain Res.* **1251,** 16–29
47. Landolt-Marticorena, C., and Reithmeier, R. A. (1994) *Biochem. J.* **302,** 253–260